Original Manuscript

Journal of
LOW FREQUENCY
NOISE, VIBRATION
AND ACTIVE CONTROL

Journal of Low Frequency Noise, Vibration and Active Control
2023, Vol. 0(0) 1–33

DOI: 10.1177/14613484231183938
journals.sagepub.com/home/lfn
Sage

An improved marine predators algorithm tuned data-driven multiple-node hormone regulation neuroendocrine-PID controller for multi-input–multi-output gantry crane system

Mohd Zaidi Mohd Tumari[1], Mohd Ashraf Ahmad[2], Mohd Helmi Suid[2], Mohd Riduwan Ghazali[2] and M Osman Tokhi[3]

Abstract

Conventionally, researchers have favored the model-based control scheme for controlling gantry crane systems. However, this method necessitates a substantial investment of time and resources in order to develop an accurate mathematical model of the complex crane system. Recognizing this challenge, the current paper introduces a novel data-driven control scheme that relies exclusively on input and output data. Undertaking a couple of modifications to the conventional marine predators algorithm (MPA), random average marine predators algorithm (RAMPA) with tunable adaptive coefficient to control the step size (*CF*) has been proposed in this paper as an enhanced alternative towards fine-tuning data-driven multiple-node hormone regulation neuroendocrine-PID (MnHR-NEPID) controller parameters for the multi-input–multi-output (MIMO) gantry crane system. First modification involved a random average location calculation within the algorithm's updating mechanism to solve the local optima issue. The second modification then introduced tunable *CF* that enhanced search capacity by enabling users' resilience towards attaining an offsetting level of exploration and exploitation phases. Effectiveness of the proposed method is evaluated based on the convergence curve and statistical analysis of the fitness function, the total norms of error and input, Wilcoxon's rank test, time response analysis, and robustness analysis under the influence of external disturbance. Comparative findings alongside other existing metaheuristic-based algorithms confirmed excellence of the proposed method through its superior performance against the conventional MPA, particle swarm optimization (PSO), grey wolf optimizer (GWO), moth-flame optimization (MFO), multi-verse optimizer (MVO), sine-cosine algorithm (SCA), salp-swarm algorithm (SSA), slime mould algorithm (SMA), flow direction algorithm (FDA), and the formally published adaptive safe experimentation dynamics (ASED)-based methods.

Keywords

Marine predator algorithms, neuroendocrine-PID, gantry crane system, metaheuristic algorithms, multi-input–multi-output system

[1]Faculty of Electrical and Electronics Engineering Technology, Universiti Teknikal Malaysia Melaka, Durian Tunggal, Malaysia
[2]Faculty of Electrical and Electronics Engineering Technology, Universiti Malaysia Pahang, Pekan, Malaysia
[3]School of Engineering, London South Bank University, London, UK

Corresponding authors:
Mohd Zaidi Mohd Tumari, Faculty of Electrical and Electronics Engineering Technology, Universiti Teknikal Malaysia Melaka, Durian Tunggal, Melaka, 76100, Malaysia.
Email: mohdzaidi.tumari@utem.edu.my

Mohd Ahsraf Ahmad, Faculty of Electrical and Electronics Engineering Technology, Universiti Malaysia Pahang, Pekan, Pahang, 26600, Malaysia.
Email: mashraf@ump.edu.my

Introduction

Effective handling of crane systems has received widespread attention in recent years due to their vast implications within container and logistic industries, centering the loading and unloading process between cargo freighters and destined harbors. Importance ultimately falls on considerably reduced freight costs, loading complexity, energy usage, complicatedness of operational mechanism, and transferrable capacity brought about by advancement of such technology.[1] Controlling a crane presents a much more intricate set of challenges compared to controlling a bridge. Unlike bridges, cranes are under-actuated systems, complex dynamics, and non-holonomic presence. This makes it exceedingly difficult to achieve precise control, even with the aid of control devices like dampers that are attached between the crane and its columns.[2,3] Particular challenge has been recognized on the transferring of payloads which exhibit oscillating and hurdling behaviors. Such has simultaneously given rise to an appealing handling issue among practitioners and control community for the development of a precise controlling mechanism which secures swifter payload transference with minimized bounce and oscillation.

Hopping on the academic bandwagon, a generous number of literature investigating the control precision of crane systems were published, which enclosed numerous control algorithms such as finite time sliding mode controller for fuzzy control,[4] H-infinity output feedback based on fuzzy model,[5] precision-positioning adaptive controller,[6] nonlinear sliding mode controls,[7] backstepping controller,[8] time-varying sliding mode control,[9] dual sliding mode control,[10] and LMI fuzzy control.[11] Upon recognizing the sole proficiency of aforementioned control schemes towards the handling of a single-input-multi-output (SIMO) crane systems by regulation of a single input (i.e., force, voltage), they have fundamentally neglected the influence of extreme coupling across disparate input channels within a real-time crane system which substantially hinders the performance robustness of implemented controller. With this in mind, proposition was set by several researchers on multi-input-multi-output (MIMO) control strategies with consideration for peripheral input channels due to their increased real-time practicality. Numerous academic endeavors were then proceeded to examine the effective handling of MIMO crane system, through investigated approaches such as enhanced-coupling nonlinear controller,[12] nonlinear adaptive tracking controller,[13] adaptive fractional-order fast terminal sliding mode with fault-tolerant control,[14] LQR controller,[15] robust tracking control using adaptive fuzzy control,[16] adaptive fuzzy control,[17] nonlinear controller embedded with an integral term,[18] and payload motion control.[19] With model-based approaches being concurrently emphasized within the literature towards designing respective controllers for both SIMO and MIMO crane systems, overwhelming efforts were especially invested to acquire the highly arduous mathematical model for each system.[20] Such attempts, nonetheless, come with the shortfalls of over reliance on a definite mathematical model towards the development of a robust controller, as well as the inability to evade issue of un-modeled dynamics amidst model simplification for controller design. Erroneous modeling ensues, whilst contributing dissatisfactory handling performance of a crane system.

On the other hand, data-driven or model-free control schemes which bypass the requirement of mathematical modeling were essentially proposed in the controlling of crane systems. Viewing the system as an unexplored black box, such approaches engage controller design by sole utilization of the input and output data.[20,21] Its simplicity has further gained considerable academic endorsement on crane system–related studies in recent years by implementing the metaheuristic optimization algorithms. This is primarily exemplified through the paper by Jaafar and Mohamed[22] in the year 2017 which proposed the implementation of PID tuning method by employment of particles swarm optimization (PSO) for the control of a nonlinear double-pendulum crane system. Having three independent PID controllers being installed towards overseeing each control variable of trolley position, hook sway, and payload oscillation, nine separate parameters were, therefore, required from the PSO algorithm within this research. An alternative approach known as adaptive differential evolutionary (ADE) algorithm was then introduced by Sun et al.[23] in the following year to optimize the given parameters of a fuzzy sliding mode anti-swing controller. Dynamic differential evolutionary (DDE) algorithm was additionally proposed within this period by the authors as a recommended single objective stochastic optimization technique to attain the optimum parameters for sliding mode controller (SMC) in elevating the performance of an under-actuated crane system.[24] Comparative study in terms of position and swing angle was further undertaken by Solihin et al.[25] in the year 2019 among the current metaheuristic-based algorithms such as PSO, cuckoo search (CS), and differential evolution (DE) towards the optimization of fuzzy controller within a gantry crane system. However, Bayesian optimizer (BO) was especially operationalized by Bao et al.[26] against the PID controller in the year 2020 for the tuning of data-driven model predictive controller (MPC) with absence of analytical model knowledge concerning the implemented crane system. Such was prior to the suggested implementation of fully informed particle swarm optimization (FIPSO) by Valluru et al.[27] within both multi-loop linear-PID and nonlinear-PID controllers of a crane system. However, the tuning of those controllers by metaheuristic optimization algorithms is still in low accuracy and need to be improved. This is because the aforementioned metaheuristic optimization algorithms have a high possibility of the solution getting stuck in local optima. Also, previously

discussed literature have merely considered the application of SIMO crane system in view of its relatively lesser tunable parameters.

In retrospect, a contemporary hybrid approach known as MFAC-PDTSFC was introduced by Roman et al.[28] in the year 2019 for the handling of a MIMO nonlinear tower crane system through the incorporation of model-free adaptive control (MFAC) to the proportional-derivative Takagi–Sugeno fuzzy controller (PDTSFC). They then proceeded with the development of first-order active disturbance rejection-virtual reference feedback tuning (ADRV-VRFT) in the ensuing year[29]; as well as the hybrid active disturbance rejection control-fuzzy controller in the year 2021,[30] targeting effectual operation of three-degree-of-freedom tower crane systems by implementing fine-tuning of the grey wolf optimizer (GWO). Whilst a MIMO crane system was applied towards these studies, the investigated model has been especially designed in parallel as a single-input–single-output (SISO) system comprising three specified domains of cart, arm angular, and payload. Moreover, employment of an enhanced model-free adaptive control (MFAC) method based on recursive least-squares (RLS) algorithm was introduced by Pham and Soffker[31] in the year 2020 to uplift the effectiveness of a MIMO-ship-mounted crane system, through a performance comparison against the projection algorithm (PA), MFAC, and proportional-integral (PI) controller. Other approaches including the data-driven neuroendocrine-PID (NEPID) control,[32,33] as well as the improved upon sigmoid-based secretion rate NEPID (SbSR-NEPID) control[34] and multiple-node hormone regulation (MnHR-NEPID) control[35] have also been proposed by Ghazali et al. for the handling of MIMO crane system. With majority of the NEPID approaches as proposed within these studies being personalized based on the adaptive safe experimentation dynamics (ASED) algorithm, the enhanced NEPID controllers as observed via latter papers have demonstrated superiority in controlling capacity over its untouched counterpart. Based on the reported data-driven control schemes above, it is evident that the majority of them utilize a metaheuristic optimization algorithm to fine-tune controller parameters. This approach has been shown to offer superior flexibility and effectiveness when applied to the control of complex crane systems. The key advantage of metaheuristic optimization algorithms is their ability to search for global optima stochastically or randomly, without requiring any gradient information. This makes it highly likely that the solutions found will avoid becoming trapped in local optima and converge to the global optimum instead. As a result, metaheuristic optimization algorithms are an excellent choice as a data-driven tool for identifying optimal controller parameters across a wide range of crane systems, delivering highly accurate trajectory control with minimal swing angle.

Among others, current advocacy is particularly allocated on the marine predators algorithm (MPA) as a contemporary metaheuristic-based algorithm for optimization of data-driven control scheme within a MIMO crane system.[36] Designed and introduced by Faramarzi et al. in the year 2020, the MPA algorithm is known for its nature-inspired metaheuristic setting which replicates the strategic foraging of ocean predators with accounts for the inter-relationship between both preys and predators. MPA stands out from other popular metaheuristic optimization algorithms due to its unique approach to balancing the tradeoff between Levy and Brownian walks. This is achieved by leveraging Levy walks to enhance the exploitation phase and Brownian walks to boost the exploration phase. Another distinguishing feature of MPA is its simple configuration, with only two coefficients requiring adjustment. In addition, the optimization process is divided into three main phases, with considerations for environmental issues and marine memory. These design elements contribute to a lower computational burden, resulting in faster convergence speeds. Due to these advantages, there is a large volume of published studies describing the role of the MPA in solving the optimization problems in various fields. For example, the MPA was used by Elminaam et al.[37] in feature selection problems to improve classification accuracy. Here, they hybrid the MPA with k-Nearest Neighbors (k-NN) called MPA-KNN to evaluate the medical dataset benchmarks. Likewise, the MPA was applied to the renewable energy sector towards fine-tuning its sensory requirement through fuzzy-logic–based maximum power point tracking (MPPT) scheme.[38] Thereafter, the algorithm was studied by Soliman et al.[39] for the appropriate extraction of electrical parameters for the triple-diode photovoltaic (TDPV) model of a photovoltaic (PV) panel. A hybrid approach between MPA and moth-flame optimization (MFO) was adopted for the optimization of multi-level threshold (MLT); in turn, boosted the image segmentation ability of CT-images against the COVID-19 pandemic.[40] Such far-reaching optimization preference is brought forward to the control engineering sector, with reviewed literature proposing the use of MPA in the tuning of cascaded proportional-integral-derivative-acceleration (PIDA) controller within interconnected power systems.[41] This has been similarly reflected in the context of infinite bus power system and IEEE-39 bus system, following the algorithm's role as an optimizer in the PID cascaded controller.[42] MPA was further regarded by Sobhy et al. as an effective optimizer in attainment of optimum PID gains for the load frequency control of modern interconnected power systems.[43] On another note, effectiveness of the algorithm was exploited as a tuning approach incorporated within the damping controller for enhanced consistency of small-signal within a high wind integrated system.[44] Previous discussion has indisputably highlighted MPA as an effective optimization approach which outshined a number of other modern metaheuristic-based algorithms, for multitude resolutions of control and operational problems in the engineering sector. Such prominence is genuinely constructed above the overshadowing convergence accuracy as yielded by the algorithm of

interest over its competing rival for majority of the benchmark functions.[36] Its potential as an excellent optimization algorithm for the control of a MIMO crane system is, therefore, justified. This is, yet, on the account of the approach's operational limitation with possessing an extreme entrapment possibility within the local optima. This is because during the transition from exploration to exploitation in Phase 2 of algorithm operationalization, each prey updates its location at each iteration only based on either its previous location or the location of the current best predator. If the location of the current best predator suddenly traps in local region, it may pull other preys to be trapped in the same region. Similarly, if the current location of the prey is suddenly trapped in the local optima region, it is difficult for it to jump out from the region since it mostly depends on the information of its previous location. Alternatively, conducted preliminary investigation has especially highlighted overly hindering nature of the existing adaptive coefficient towards step size control (defined as *CF*),[36] which undermined MPA's proficiency in the balancing of exploration and exploitation phases. Therefore, the implementation of an unadjusted MPA algorithm in a MIMO crane system would merely generate subpar control performance.

Tackling the emerged shortfalls of MPA, random average marine predators algorithm (RAMPA) with tunable adaptive coefficient for the controlling of step size (*CF*) is hereby proposed. The introduced algorithm consisted RAMPA as its principal component which capitalizes computation of random average between both the current preys' and the current best predator's locations to confront local optima issue during Phase 2 of algorithm operationalization. Specifically, both of prey and predator within the outlier could avert their respective entrapments by assistance from both current best predator and current preys. Peripheral component of the proposed algorithm further comprised tunable *CF* to improve a balance between exploration and exploitation phases. Set to overcome the restrictive nature of MPA, increased flexibility is enabled via the proposed method towards maintaining a balanced exploration and exploitation phases; in which, cumulatively encourages searching competency.

Based upon the given arguments, random average marine predators algorithm (RAMPA) with tunable adaptive coefficient for controlling the step size (*CF*) has been strategically unveiled within this paper for the fine-tuning of data-driven multiple-node hormone regulation of neuroendocrine-PID (MnHR-NEPID) within a MIMO gantry crane system. Such step is taken to exploit the algorithm advantage of resolving local optima entrapment, as well as the issue of unbalanced segregation between the exploration and exploitation phases. Replicated upon the reported work in refs. 34,35, the MnHR-NEPID controller is particularly chosen for its overpowering precision and synergy between multiple nodes hormones, over a standard NEPID controller and the SbSR-NEPID in the controlling of the specified MIMO system. With ASED algorithm as proposed in the earlier paper being founded upon both local search principle and an extreme reliance on feasible selection of initial control parameters, an indefinite global optimal solution from said algorithm has fundamentally propelled consecutive investigation of RAMPA-based method with tunable *CF* towards similar research circumstance. Assessments are further made in regards to the convergence curve and statistical analysis of fitness function, the total norm of error and the total norm of input, findings as obtained from the Wilcoxon's rank test, time responses, followed by performance appraisal in the presence of external disturbance. Statistical comparison is consequently attempted alongside the conventional MPA, as well as other preceding algorithms including PSO, GWO, MFO, multi-verse optimizer (MVO), sine-cosine algorithm (SCA), salp-swarm algorithm (SSA), slime mould algorithm (SMA), and flow direction algorithm (FDA). Additionally, the ASED-based method as examined in ref. 35 has been especially measured against the proposed algorithm in pursue of the superior approach. Key contributions of the current work, thus, include:

(i) A random average location calculation is proposed in RAMPA, which will help the MPA to escape from the local optima. The merit of the random average location between prey and current best predator is that the location of the current best predator or the location of the current prey can help any trapped prey or predator to jump out from the local optima region and continue a new search track.
(ii) Search competency of the conventional MPA is improved ensuing incorporation of tunable *CF* which permits greater users' freedom or flexibility towards balance in exploration and exploitation stages.
(iii) The current study essentially pioneered the implementation of multi-agent–based optimization (i.e., RAMPA based method with tunable *CF*) for the fine-tuning of MnHR-NEPID controller. Results as registered from the proposed algorithm further dominated its significant excellence over other recent multi-agent–based methods, such as FDA, SMA, SSA, and MVO.

The remaining sections of this paper are coordinated as follows: The second section specifies on discussion of the conventional MPA-based method and the contemporarily proposed RAMPA-based method with tunable *CF*. The third section is then purposed for problem formulation concerning employment of the MnHR-NEPID controller within a MIMO gantry crane system, followed by the systematic outlining of required procedure towards employment of the proposed

method for performance optimization. Effectiveness of the proposed method is further validated in the fourth section. Last but not least, concluding remarks concerning the entire research are given in the fifth section.

Improved marine predators algorithm

The current section sets to explain improvements made towards the conventional marine predators algorithm (MPA) for the tuning of MnHR-NEPID controller within a MIMO gantry crane system. Herewith, the conventional MPA-based algorithm has been initially interpreted and described. Discussion is then given on the RAMPA-based method with tunable *CF* as per contemporarily introduced within this paper.

Review of the marine predators algorithm

Academically founded by Faramarzi et al.,[36] marine predators algorithm (MPA) transpires a predator-inspired algorithm that upholds the *survival of the fittest* within the ocean environment towards achieving the utmost optimal strategy amid food foraging. Such food foraging phenomena commonly reviews the random walk strategies of ocean predators enclosing both the Levy and Brownian walks. Levy walk which is drawn from a probability function based on power-law tail has a characteristic of many small steps associated with longer relocations. It is usually employed for foraging prey with less concentration.[45] Meanwhile, the Brownian walk consists of step length drawn from a probability function based on Normal (Gaussian) distribution which is utilized to search in prey-abundant areas.[45] MPA, thus, intends to acquire the most optimized strategy through reaching an equalized compromise between both the Levy and Brownian strategies. In MPA, the predator is foraging for the food as well as the prey is foraging for its food.

Operationalization of MPA is primarily established on the random distributed of initial solutions for both preys and predators across the provided search space in seek of resolving the given optimization issue

$$arg \min_{X_i(1), X_i(2)\ldots} f_i(X_i(k)) \tag{1}$$

for iterations $k = 1, 2, \ldots, k_{max}$, where the fitness function of agent i is being represented by f_i, the position vector of agent i is being represented by X_i, with the maximum number of iterations being represented by k_{max}. Having the search agents being denoted by both preys and predators, definitions of the two main matrices including elite matrix E which comprises the best predators and prey matrix P which comprises the preys are necessarily obtained. Definitions of both the elite matrix and prey matrix are, thus, written as

$$E = \begin{bmatrix} X'_{1,1} & X'_{1,2} & \cdots & X'_{1,d} \\ X'_{2,1} & X'_{2,2} & \cdots & X'_{2,d} \\ \vdots & \vdots & \vdots & \vdots \\ X'_{n,1} & X'_{n,2} & \cdots & X'_{n,d} \end{bmatrix}, \tag{2}$$

$$P = \begin{bmatrix} X_{1,1} & X_{1,2} & \cdots & X_{1,d} \\ X_{2,1} & X_{2,2} & \cdots & X_{2,d} \\ \vdots & \vdots & \vdots & \vdots \\ X_{n,1} & X_{n,2} & \cdots & X_{n,d} \end{bmatrix}, \tag{3}$$

where the total number of agents and dimensions are independently represented by the symbols n and d. In enabling increased clarity and understanding, let $X'_{i,j}$ in equation (2) be the j-th element of the best predator vector X'_i, which are replicated n times in the matrix E. In this case, X'_i is chosen from the best position vector among the search agent in each iteration. Moving forward with equation (3), $X_{i,j}$ presents the j-th dimension of i-th prey or agent X_i in equation (1). Both the predators and preys are then updated based on three main phases as well as the environmental issues and marine memory to find the global optimum solution. Details regarding the MPA structure are further described as follows:

Phase 1: Exploration phase. Acknowledging faster motions among the preys in Phase 1, such occurrence signals active food foraging attempts within the prey against its more linger predator counterpart with little to no motion. Such circumstance is

apparent for first tierce of the maximum iterations (k_{max}) ensuing full commencement of the exploration stage. Positions of the preys are subsequently revised by employing the following equation

$$P_i = P_i + Q.r_1 \otimes \left[R_B \otimes (E_i - R_B \otimes P_i)\right], \text{if } k < \frac{1}{3}k_{max}, \tag{4}$$

for $i = 1, 2, \ldots, n$. As observed in equation (4), P_i and E_i represent the i-th row of matrices P and E, respectively, with vector of random numbers for the Brownian motion being further represented by R_B. The element-wise multiplications is then signified by the notation $\otimes$, with Q being a constant number which has been predetermined at a value of 0.5 and r_1 being a random number as withdrawn from uniform distribution across the range of [0, 1].

Phase 2: Transition from exploration to exploitation phase. Both the predators and preys are maneuvering at similar rate in Phase 2. Such occurrence symbolizes a deviation within the prey with perturbation of a subgroup approaching the exploitation stage and the locational update of the other subgroup as rooted by motions of the predators approaching the exploration stage. Known for being a transitional process between both exploration and exploitation stages, motions of the involved agents equally differ based on their exploration intention within the Brownian walk and the exploitation intention within the Levy walk. Happened between one third to two third of k_{max}, updated positions of the prey for $i = 1, 2, \ldots, n/2$ are, therefore, acquired through the equation

$$P_i = P_i + Q.r_1 \otimes [R_L \otimes (E_i - R_L \otimes P_i)], \text{if } \frac{1}{3}k_{max} < k < \frac{2}{3}k_{max}, \tag{5}$$

with updated positions for $i = n/2, n/2 + 1, \ldots, n$ being further given by

$$P_i = E_i + Q.CF \otimes [R_B \otimes (R_B \otimes E_i - P_i)], \text{if } \frac{1}{3}k_{max} < k < \frac{2}{3}k_{max}. \tag{6}$$

Random number based on the Levy distribution in equation (5) is hereby given by R_L, whilst having random number based on the Brownian distribution and adaptive coefficient that controls step size of the predator motion in equation (6) being, respectively, given by R_B and CF. The expression of CF is then detailed as per follows

$$CF = \left(1 - \frac{k}{k_{max}}\right)^{\left(2 \times \frac{k}{k_{max}}\right)}. \tag{7}$$

Phase 3: Exploitation phase. Phase 3 of the MPA structure further demonstrates a faster motion by the predators. Such overshadowing pace against motion rate of the prey, thus, signifies increased exploitation. Such execution especially occurs at the final tierce of maximum iteration k_{max} ensuing the predators' operationalization within the Levy walk. Consideration is subsequently placed on the synergy between each prey and the predators at an increased mobilizing pace for $i = 1, 2, \ldots, n$, with respective locational updates that follows the equation

$$P_i = E_i + Q.CF \otimes \left[R_L \otimes (R_L \otimes E_i - P_i)\right], \text{if } k > \frac{2}{3}k_{max}. \tag{8}$$

Eddy formation or fish aggregating devices' effect. Beyond the three principle phases of MPA as discussed previously lies fundamental interest for the behavioral endeavors of ocean predators facing various circumstantial conditions known as the eddy formation or fish aggregating devices (*FADs*) effect. Amidst the predators' food hunting process within domains of the Levy and Brownian walks, aspiration to reach a location with bountiful preys in the vast ocean would motivate an extensive vertical leap and dive. Such attempt would ultimately prevent stagnating of the predators' within the local optima. Nevertheless, effect of the *FADs* is written as per the equation

$$P_i = \begin{cases} P_i + CF[LB + r_1 \otimes (UB - LB)] \otimes U, \text{if } r_2 \leq FADs, \\ P_i + [FADs(1 - r_2) + r_2](P_{r_3} - P_{r_4}), \text{if } r_2 > FADs, \end{cases} \tag{9}$$

where $FADs = 0.2$, with values as randomly generated between the range of [0, 1] being denoted by r_1 and r_2, and the upper and lower bound vectors being denoted by UB and LB, respectively. U is hereby given as the symbol that represents a binary

vector with elements comprising the values of 0 and 1. On this note, a zero array shall be generated by U in the case where $r_2 \leq 0.2$, vice versa. However, random indexes for column of the prey matrix are given by the symbols of r_3 and r_4.

Marine memory. Additional characteristic of MPA forwarded the structural capacity to retain and remember particular positions with immense foraging activities among the predators towards evading local solutions. Emphasis is brought to the appraisal of fitness for every prey towards updating of the elite matrix E following revision of the prey matrix P and operationalization of the *FADs* effect. Comparison is hereby executed between fitness of each solution for the current iteration and the equivalence from the previous iteration. Replacement would then occur shall the current solution is deemed more feasible or well-fitted as a superior stand-in to the antecedent. The mechanism entirely simulates return of the predators to their successful high production foraging area. With this in mind, marine memory is, therefore, undertaken for quality improvement of acquired solution from the entire involved iterations.

A detailed explanation of MPA can be further obtained via ref. 36.

Random average marine predators algorithm with tunable CF

While MPA demonstrates robust performances and functionalities in overcoming a vast range of optimization problems, shortfalls of the algorithm are observed from its crippled competency to withdraw from the local optima is weakened under certain circumstances, as well as an inadequate balance between both exploration and exploitation phases upon tackling specified optimization problems. Modifications are, therefore, proposed on the conventional MPA method to resolve the previously mentioned stagnation issue within the local optima, whilst enhancing offsetting potential between both the exploration and exploitation phases.

Random average location of preys in updating mechanism. Particular deficiency of the conventional MPA method has been recognized on inability of the current best predator to withdraw from the local optima region. As the earlier discussed Phase 2 of the algorithm clearly highlights the revising of preys' updated positions above the ground of its previous location or location of the current best predator, trapping of the current best predator could possibly guide its preys into its current local optima region. Previous position of prey which failed to escape the local optima region would further define its consequential position at the same location. Such issue is deemed solvable by incorporating the random average between current positions for both the preys and the best predators to the structure's updating mechanism. With the computation of random average being undertaken within individual iteration, any particular criteria for the process are, therefore, dismissed. Adoption of random average is hereby advantageous due to the competencies of current best predators and current preys in aiding the escape of trapped best predators and prey from the local optima region; in turn, enabling their subsequent exploration of contemporary search domains. Operationalization of the structure's Phase 2, thus, encompasses revising of the preys' consecutive positions through the computation of individual element's random average. Such process is further described as per the equation

$$RA_{i,j} = P_{i,j}(1 - r_5) + E_{i,j}.r_5. \tag{10}$$

As outlined in equation (10), $RA_{i,j}$ presents random average for current element of the prey's location $P_{i,j}$, and current element of the best predator's location $E_{i,j}$ for j-th dimension of i-th prey. In this case, an element for both P_i and E_i is especially given by $P_{i,j}$ and $E_{i,j}$, respectively. A random number as evenly segregated within the range of [0, 1] is then denoted by r_5. Following the adoption of equation (10) into both equation (5) and equation (6), the equations for RAMPA are contemporarily revised for $i = 1, 2, \ldots, n/2$ as

$$P_i = RA_i + Q.r_1 \otimes [R_L \otimes (E_i - R_L \otimes P_i)], \text{if } \frac{1}{3}k_{max} < k < \frac{2}{3}k_{max}, \tag{11}$$

with the equation for $i = n/2, n/2 + 1, \ldots, n$ being subsequently written as

$$P_i = RA_i + Q.CF \otimes [R_B \otimes (R_B \otimes E_i - P_i)], \text{if } \frac{1}{3}k_{max} < k < \frac{2}{3}k_{max}, \tag{12}$$

where RA_i is a vector that consists of element $RA_{i,j}$ in equation (10).

Graphical illustration for a pre-established contour plot comprising a two-dimensional location ($d = 2$) has been presented in Figure 1 in ensuring greater clarification concerning RAMPA's objective. Under the circumstance where the current best predator E_i (blue circle) is unexpectedly entrapped within the local optima amidst operationalization of Phase 2,

employment of a conventional MPA approach would present an immerse possibility where E_i retains its trapped position, whilst worsening the situation shall drag the prey P_i (red circle) consequently towards the same location. Despite absence of graphical illustration for equation (5), similar circumstance would prevail for the equation following a lofty percentage where the current prey P_i would be entrapped within the local optima region, whilst its continuous probe for alternative search track may be jeopardized. Represented by RA_i (green circle) via Figure 1, the complication as encountered in both cases is, nonetheless, solvable through the employment of random average between both E_i and P_i within the updating mechanism.

Normal average, as introduced by Jui and Ahmad,[46] capitalizes distance of the average location as a constant center to both the current and the current best locations. However, such execution fails to replicate the stochastic nature of both prey and predator motions. Towards offering an increased motional variations, a different approach has been proposed within the random average method by randomizing distance of the random average location based on the random number r_5. Under the condition where r_5 is 0.5, the distance of RA_i would center between P_i and E_i. Under the condition where r_5 is greater than 0.5, the distance of RA_i would be randomized closer to P_i. Under the condition where r_5 is smaller than 0.5, the distance of RA_i would then be randomized closer to E_i. The resultant RA_i as acquired from such operation would inevitably possess increased capacity for the withdrawal of trapped E_i or P_i towards their ensuing exploration at other regions for better solution.

Tunable adaptive coefficient for controlling the step size. The tunable adaptive coefficient as proposed to control the step size (*CF*) has been further elaborated within the current section. Herewith, improvement can be particularly made to the both the exploration and exploitation phases of the conventional MPA through adjusting the current *CF*. Contradicted in nature, an overwhelmed exploration would compromise the precision of global optimum value, with an overwhelmed exploitation being the direct antecedent to stagnation issue within the local optima. Nevertheless, executed constraint to *CF* within Phase 2, Phase 3, and *FADs* for the structure of a conventional MPA-based method would dominate an unacceptable balance between both exploration and exploitation. Such is observable through equation (7) where having the value of *CF* being nonlinearly reduced from 1 to 0 has proven overly prohibitive to allow users' resilience in controlling and manipulation of both the exploration and exploitation phases. Concern as presented on the limitation imposed by the existing *CF* towards the operationalization of MPA is then justified on the need for a more universalized equation admissible to a vaster range of applications. Therefore, a tunable or adjustable *CF* can be employed to the currently studied algorithm for increased freedom in maintaining an offsetting balance between both exploration and exploitation. In seek of greater search competency, the equation of *CF* within equation (7) is, thus, revised and written as

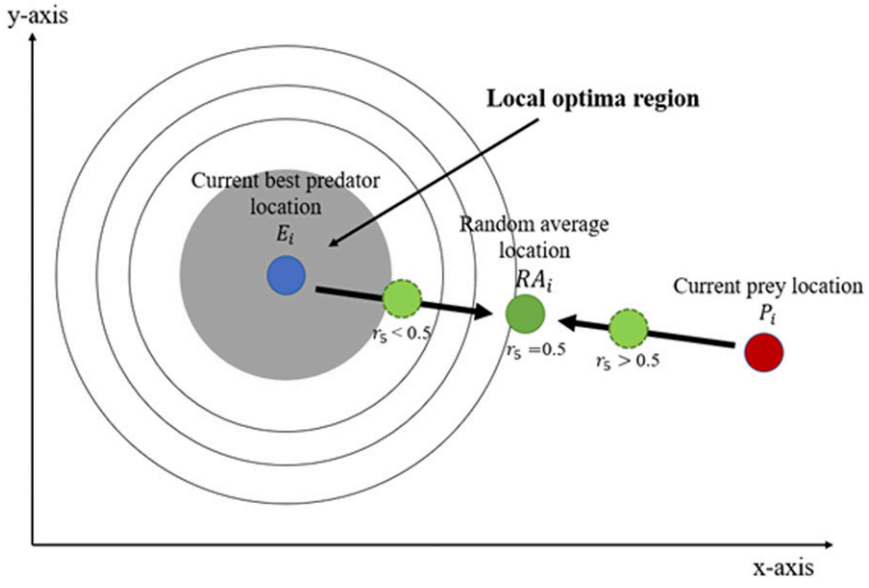

Figure 1. Graphical representation of the random average location mechanism.

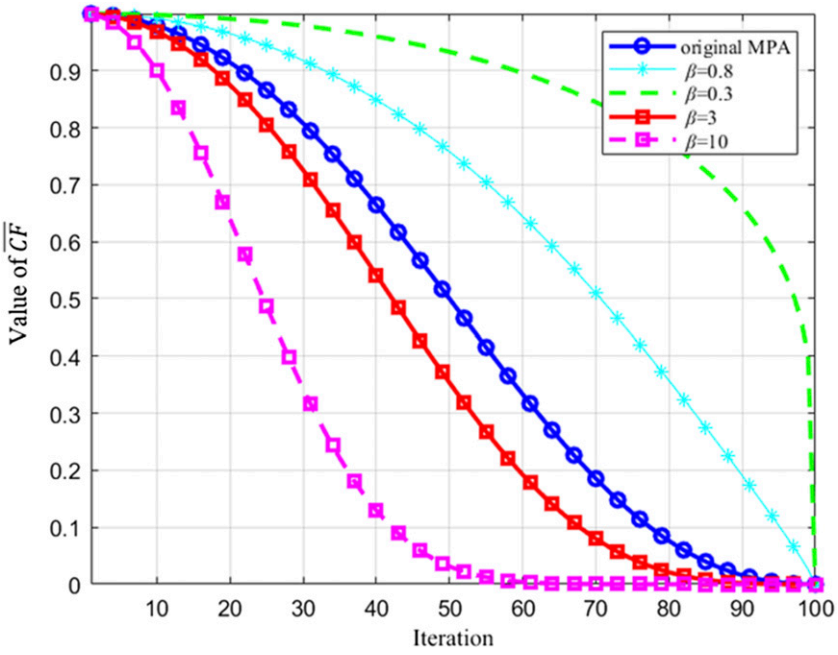

Figure 2. Value of $\overline{CF}$ for different β.

$$\overline{CF} = \left(1 - \frac{k}{k_{max}}\right)^{\left(\beta \times \frac{k}{k_{max}}\right)}, \tag{13}$$

where the contemporarily introduced coefficient as tunable towards adjusting the ratio of both exploration and exploitation phases under the tuning process is being given by β. With this in place, expectation especially falls on the employment of RAMPA-based method with tunable CF as an enhanced alternative towards an increasingly promising performance in the optimization of MnHR-NEPID controller for a MIMO gantry crane system. Additional benefit in the form of increased ratio options between both exploration and exploitation phases would also enable the algorithm's greater compatibility to a wide extent of real-time optimization problems as compared to its unmodified predecessor. Flexibility as offered by the proposed RAMPA-based method with tunable CF would then trace the procedure of a conventional MPA through the substitution of $\overline{CF}$ in equation (13) to the CF in equation (8), equation (9), and equation (12). The implication for varying values of β against value of the proposed $\overline{CF}$ has been further illustrated in Figure 2. As observed, an increased exploitation capacity can be achieved in the case where β can be set greater than 2, for example, $\beta = 10$. Conversely, an increased exploration capacity can be achieved upon setting β to lower value than 2, for example, $\beta = 0.3$. As such, pseudocode for the proposed RAMPA-based method with tunable CF has been systematically outlined in **Algorithm 1**.

Algorithm 1. Proposed RAMPA with tunable CF algorithm

1. Initialize UB, LB, $k_{max}, n, d, Q, FADs$, and β
2. Randomly initialize the search agents P_i populations $i = 1, 2, \ldots, n$
3. $k = 1$
4. **While** $k < k_{max}$
5. Evaluate the fitness of all P_i, followed by construction of the E_i matrix and accomplishing of the memory saving
6. **If** $k < \frac{1}{3} k_{max}$
7. Update P_i based on equation (4)
8. **Else if** $\frac{1}{3} k_{max} < k < \frac{2}{3} k_{max}$
9. Within first half of the populations $(i = 1, 2, \ldots, n/2)$
10. Update P_i based on equation (11)

11. Moving forward to second half of the populations $(i = n/2, n/2 + 1, \ldots, n)$
12. Update P_i based on equation (12) by employing CF from equation (13)
13. **Else if** $k > \frac{2}{3}k_{max}$
14. Update P_i based on equation (8) by employing CF from equation (13)
15. **End (if)**
16. Evaluate memory saving, followed by the updating of E_i
17. Applying *FADs* effect and update based on equation (9) by employing CF from equation (13)
18. **End while**

Having the above explanation as a basis, the proposed revision to the conventional MPA algorithm can be segregated into two separate segments. The first segment hereby focuses equal allocation of the population towards both the exploitation and exploration phases amidst Phase 2 of the MPA structure. Extreme velocity exerted by both the involved preys and predators during this phase would cause an upsurge in the best predators' and the preys' possibilities of missing the global optima; whilst, entailing failure in avoiding the local optima region. A random average location is, therefore, employed within a conventional MPA towards offsetting agile nature of the involved agents, whilst enabling reciprocated corporations between the existing preys or predators and their outlier counterparts to escape the local optima region for continuous exploration of new search space. As opposed to the correlation in Phase 1, notable superiority in velocity of the preys as compared to the predators has propelled the prey for the exploration of other search spaces and maneuver within the Brownian walk as the most active agents, with the predators standing by for the preys' locations. Following the preys' continuous searching process that diminishes their potential entrapment within the local optima, such reasoning, therefore, justified impertinence of the proposed random average calculation within Phase 1. Similar situation is reflected for Phase 3, in which increased capacity towards preys' exploitation by predators' that maneuver within the Levy walk would have diminished the credit of random average calculation. Such endeavor as implemented during the previous phase has fundamentally enhanced the avoidance capacity of preys' from their entrapment within the local optima. On another note, tunable CF would then be applied solely within Phase 2, Phase 3, and *FADs* of the structure. With the predators maneuvering in Brownian manner amidst second half of Phase 2's populations, tunable CF is hereby implemented to secure the opportunity of manipulating the predators' step size towards equalizing both exploration and exploitation. In the accounts of Phase 3 which capitalizes heightened exploitation, a shift in the predators motions towards the Levy walk does not entirely overshadow the possibility of step size control in seek of enhancing the agents' search capacity across global optimum. However, employment of a tunable CF within *FADs* would further allow a divergence of vertical leaps among predators with the aim of discovering other promising domains with bountiful preys. Discussed proposition has, nonetheless, displayed thorough expectation on an improved operationalization of the conventional MPA through both an enhanced local optima avoidance and an eminent balance between the exploration and exploitation phases.

Improved marine predators algorithm tuned data-driven multiple-node hormone regulation neuroendocrine-PID controller of multi-input–multi-output gantry crane system

Modeling of the multi-input–multi-output (MIMO) gantry crane system is initially described in the current section. Explanation ensues on the problem formulation of multiple-node hormone regulation neuroendocrine-PID (MnHR-NEPID) controller for MIMO gantry crane system. Application of random average MPA (RAMPA) based method with tunable CF towards the tuning of MnHR-NEPID controller for MIMO gantry crane system is further described.

Modeling of multi-input–multi-output gantry crane system

Replicated based on a real-time gantry crane system, this study particularly employs the multi-input–multi-output (MIMO) gantry crane model as proposed by Park et al..[47] The structure has been outlined in Figure 3 in which swinging motions of the payload is accomplished through maneuvering of the trolley. Both directions of the trolley's horizontal maneuver and the rope's vertical course are individually denoted by the X-axis and Z-axis, respectively. Control input used to mobilize the trolley in its horizontal course is further denoted by $F_x(t)$, with the control input towards the hoist in the l-direction being further denoted by $F_l(t)$. However, recorded outputs with respect to the sway angles of payload, rope length, and trolley

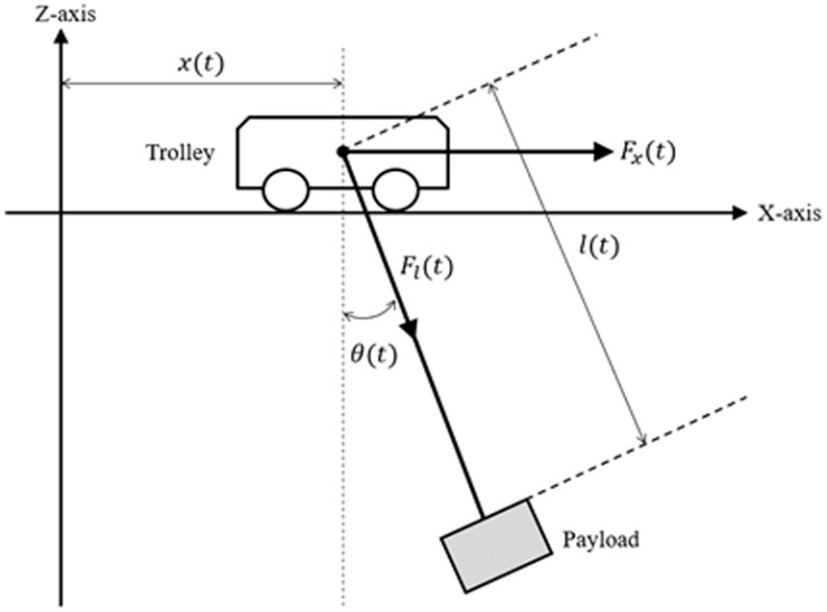

Figure 3. The container gantry crane system.

displacement are represented by $\theta(t)$, $l(t)$, and $x(t)$, independently. The equations enclosing motions of the studied gantry crane system are, therefore, described as per the following

$$\dot{\boldsymbol{x}}_a = \begin{bmatrix} \dot{\boldsymbol{q}} \\ -M^{-1}(\boldsymbol{q})[W_m(\boldsymbol{q},\dot{\boldsymbol{q}})\dot{\boldsymbol{q}} + R(\dot{\boldsymbol{q}})] \end{bmatrix} - \begin{bmatrix} 0_{3\times3} \\ -M^{-1}(\boldsymbol{q}) \end{bmatrix} \begin{bmatrix} 1 & 0 & 0 \\ 0 & 1 & 0 \end{bmatrix}^T \boldsymbol{u}_a, \tag{14}$$

where $\dot{\boldsymbol{x}}_{a6\times1} = \begin{bmatrix} x & l & \theta & \dot{x} & \dot{l} & \dot{\theta} \end{bmatrix}^T$, $\boldsymbol{u}_{a2\times1} = [u_1 \quad u_2]^T = [F_x \quad F_l]^T$, $\boldsymbol{q}_{3\times1} = [x \quad l \quad \theta]^T$

$$M(\boldsymbol{q})_{3\times3} = \begin{bmatrix} m_p + m_t & m_p sin\theta & m_p lcos\theta \\ m_p sin\theta & m_p + m_l & 0 \\ m_p lcos\theta & 0 & m_p l^2 + I \end{bmatrix}, \tag{15}$$

$$W_m(\boldsymbol{q},\dot{\boldsymbol{q}})_{3\times3} = \begin{bmatrix} 0 & m_p\dot{\theta}cos\theta & -m_p lsin\theta\dot{\theta} + m_p cos\theta\dot{l} \\ 0 & 0 & -m_p l\dot{\theta} \\ 0 & m_p l\dot{\theta} & m_p l\dot{l} \end{bmatrix}, \tag{16}$$

and

$$R(\dot{\boldsymbol{q}})_{3\times1} = [0 \quad -m_p gcos\theta \quad m_p glsin\theta]^T. \tag{17}$$

Thereafter, acquired output for the container gantry crane would be given as

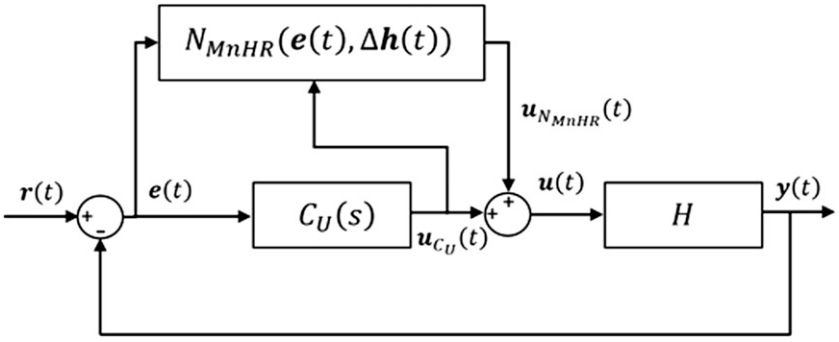

Figure 4. The MnHR-NEPID control system.

$$\boldsymbol{y} = \begin{bmatrix} 1 & 0 & 0 & 0 & 0 & 0 \\ 0 & 1 & 0 & 0 & 0 & 0 \\ 0 & 0 & 1 & 0 & 0 & 0 \end{bmatrix} \begin{bmatrix} x \\ l \\ \theta \\ \dot{x} \\ \dot{l} \\ \dot{\theta} \end{bmatrix} = \begin{bmatrix} x \\ l \\ \theta \end{bmatrix} = \boldsymbol{q}. \tag{18}$$

Adopted directly from ref. 47, $m_p = 0.73$ kg, $m_t = 1.06$ kg, $m_l = 0.5$ kg, and $I = 0.005$ kgm^2 are further established as key parameters to the currently studied gantry crane system.

Problem formulation

This section is especially allocated to the formulation of problem concerning synthesis of MnHR-NEPID control towards the MIMO gantry crane system as previously described in Section 3.1. In accordance to the report by ref. 35, the block diagram of MIMO gantry crane system as controlled using MnHR-NEPID has been detailed in Figure 4, with the reference, control input and output measurement being individually represented by $\boldsymbol{r}(t) \in \mathbb{R}^q$, $\boldsymbol{u}(t) \in \mathbb{R}^p$ and $\boldsymbol{y}(t) \in \mathbb{R}^q$, respectively. Both dimensions of the control input $\boldsymbol{u}(t)$ and the output measurement $\boldsymbol{y}(t)$ are further denoted by independent symbols of p and q.

As shown, the MnHR-NEPID controller comprising both a PID controller unit $C_U(s)$ and the multiple-node hormone regulation of neuroendocrine controller $N_{MnHR}(\boldsymbol{e}(t), \Delta\boldsymbol{h}(t))$, is connected preceding the MIMO gantry crane system as denoted by H. Herewith, $C_U(s)$ as employed to control the given MIMO gantry crane system is described as

$$C_U(s)_{p\times q} = \begin{bmatrix} C_{11}(s) & \cdots & C_{1q}(s) \\ \vdots & \ddots & \vdots \\ C_{p1}(s) & \cdots & C_{pq}(s) \end{bmatrix}, \tag{19}$$

where

$$C_{ij}(s) = K_{Pij}\left(1 + \frac{1}{K_{Iij}s} + \frac{K_{Dij}s}{1 + \left(K_{Dij}/N_{ij}\right)s}\right). \tag{20}$$

The PID controller for $i = 1, 2, \ldots, p$ and $j = 1, 2, \ldots, q$ is further represented by $C_{ij}(s)$ in equation (20), with the proportional gain, integral time, derivative time, and filter coefficient being independently represented by $K_{Pij} \in \mathbb{R}$, $K_{Iij} \in \mathbb{R}$, $K_{Dij} \in \mathbb{R}$, and $N_{ij} \in \mathbb{R}$. Moving forward, acquired output $C_U(s)$ for the MIMO gantry crane system is subsequently expressed by

$$\boldsymbol{u}_{C_U}(t) = \left[\sum_{j=1}^{q} h_{1j}, \quad \sum_{j=1}^{q} h_{2j}, \quad \cdots \quad \sum_{j=1}^{q} h_{pj} \right]^T, \tag{21}$$

where the output individual C_{ij} and the error of individual output plant H are given by $h_{ij} = C_{ij}(s)e_j(t)$ and $e_j(t) = r_j(t) - y_j(t)$, respectively. Following this, the expression for $N_{MnHR}(\boldsymbol{e}(t), \Delta\boldsymbol{h}(t))$ is then written as follows

$$N_{MnHR}(\boldsymbol{e}(t), \Delta\boldsymbol{h}(t))_{p\times q} = \begin{bmatrix} Y_{V_{11}} & \cdots & Y_{V_{1q}} \\ \vdots & \ddots & \vdots \\ Y_{V_{p1}} & \cdots & Y_{V_{pq}} \end{bmatrix}, \tag{22}$$

where

$$Y_{V_{ij}} = \left(1 - \eta_j\right) V_{ij} + \eta_j \left(\sum_{k=1}^{p} \sum_{\iota=1}^{q} V_{k\iota} \right), \tag{23}$$

for $i = 1, 2, \ldots, p$ and $j = 1, 2, \ldots, q$. Note that, $V_{k\iota}$ has been devoted to remark all existing nodes of hormone regulation within the neuroendocrine controller. Moving forward, single node of the neuroendocrine controller is subsequently given as

$$V_{ij}\left(e_{ij}(t), \Delta h_{ij}(t)\right) = \alpha_{ij} \left[\frac{\left|\Delta h_{ij}(t)\right|^{\zeta_{ij}}}{\lambda_{ij} + \left|\Delta h_{ij}(t)\right|^{\zeta_{ij}}} + \rho_{ij} \right] L_1 L_2, \tag{24}$$

where $i = 1, 2, \ldots, p$ and $j = 1, 2, \ldots, q$, $\Delta h_{ij}(t) = h_{ij}(t) - h_{ij}(t - t_s)$ and $\Delta e_j(t) = e_j(t) - e_j(t - t_s)$. The sampling time for $t = t_s, 2t_s, 3t_s, \ldots, ct_s$ is further denoted by t_s at the number of samples c. The hill coefficient of each hormone is denoted by ζ_{ij}, with the constant positive real numbers being, respectively, represented by ρ_{ij} and λ_{ij}. The direction factors of neuroendocrine are then denoted by the symbols L_1 and L_2. With adherence to the criterion where $V_{ij}(e_{ij}(t), \Delta h_{ij}(t)) = 0$ when $\Delta h_{ij}(t) = 0$; ρ_{ij} is, therefore, entirely specified to the value of 0. The description of equation (24) has been thoroughly detailed in ref. 32; multiple-node switching mechanism η_j has further been deliberated as per the following

$$\eta_j = \begin{cases} 0, & \text{if } -T_h \le e_j(t) \le T_h, \\ G\left(e_j\right), & \text{if } -T_h > e_j(t) > T_h, \end{cases} \tag{25}$$

where the error threshold and control variable error of each j output response are being independently represented by T_h and e_j. Attention is hereby acknowledged on the selection of T_h in accordance to the system's settling time that falls within the span of 2% to 5% of the final value. The normalized Gaussian function $G(e_j)$ is described based on the equation

$$G\left(e_j\right) = 1 - exp\left(\frac{-\left(e_j - \mu_{ij}\right)^2}{2\sigma_{ij}^2} \right), \tag{26}$$

where both the variance and the center vector of ij node are being independently represented by σ_{ij}^2 and μ_{ij}. Upon ensuring the normalized Gaussian function is centralized at zero value, the value of μ_{ij} is correspondingly determined at 0 towards ascertaining both positive and negative error of the control variable e_j. On the accounts where an inverse normalized Gaussian function ranged between the values of 0 and 1 is especially adopted for the current study, acquired output for the function would, therefore, progress approaching the value of 1 to secure a greater control variable error $e_j(t)$. Such outcome would bring about high multiple-node switching mechanism for the hormone regulation η_j.

Output as obtained from $N_{MnHR}(\boldsymbol{e}(t), \Delta\boldsymbol{h}(t))$ has further been represented by

$$\boldsymbol{u}_{N_{MnHR}}(t) = \left[\sum_{j=1}^{q} Y_{V_{1j}}, \quad \sum_{j=1}^{q} Y_{V_{2j}}, \quad \cdots \quad \sum_{j=1}^{q} Y_{V_{pj}} \right]^T. \tag{27}$$

On this account, total output as obtained from the MnHR-NEPID controller $\boldsymbol{u}(t)$ is, thus, given as

$$\boldsymbol{u}(t) = \boldsymbol{u}_{C_U}(t) + \boldsymbol{u}_{N_{MnHR}}(t), \tag{28}$$

where $\boldsymbol{u}(t)_{p\times 1} = [u_1(t), u_2(t), \ldots, u_p(t)]^T$, $\boldsymbol{u}_{C_U}(t) \in \mathbb{R}^p$, and $\boldsymbol{u}_{N_{MnHR}}(t) \in \mathbb{R}^p$.

Performance of the MIMO gantry crane system handled using the MnHR-NEPID controller in Figure 4 is then assessed based on the performance index as outlined in the following equations

$$\overline{e}_j := \int_{t_0}^{t_f} \left| r_j(t) - y_j(t) \right|^2 dt, \tag{29}$$

$$\overline{u}_i := \int_{t_0}^{t_f} |u_i(t)|^2 dt, \tag{30}$$

where the respective j-th elements of vectors $\boldsymbol{r}(t)$ and $\boldsymbol{y}(t)$ are individually denoted by $r_j(t)$ and $y_j(t)$, with the i-th elements of vector $\boldsymbol{u}(t)$ being further denoted by $u_i(t)$. At $t_0 \in \{0\} \cup \mathbb{R}_+$ and $t_f \in \mathbb{R}_+$, the duration involved to assess the system's performance is given by an interval of $[t_0, t_f]$. In order to optimize the system's performance, we have carefully chosen a set of performance indices. Our primary objective is to reduce the tracking error, which is essentially the deviation between the reference inputs $\boldsymbol{r}(t)$ and the actual output measurements $\boldsymbol{y}(t)$ (such as the sway angles of the payload, rope length, and trolley displacement). Additionally, we are also taking into consideration the energy required for the control inputs $\boldsymbol{u}(t)$, striving to minimize it as much as possible. This approach ensures that the system operates with maximum efficiency and accuracy, delivering superior results. The application of these performance indices has garnered widespread acclaim among researchers, who have lauded their ability to enhance the accuracy of gantry crane systems. Indeed, their efficacy has been validated in numerous studies, such as those cited in refs. 34,35.

Furthermore, fitness function which will be used for the data-driven tuning of MnHR-NEPID controller within the MIMO gantry crane system is given by

$$J\left(\boldsymbol{K_P}, \boldsymbol{K_I}, \boldsymbol{K_D}, \boldsymbol{N}, \boldsymbol{\zeta}, \boldsymbol{\lambda}, \boldsymbol{\alpha}, \boldsymbol{\sigma^2}\right) = \sum_{j=1}^{q} w_{1j}\overline{e}_j + \sum_{i=1}^{p} w_{2i}\overline{u}_i, \tag{31}$$

where parameters of the MnHR-NEPID controller for the studied MIMO gantry crane system are stated at $\boldsymbol{K_P} := [K_{P_{11}}, K_{P_{12}}, \ldots, K_{P_{pq}}]$, $\boldsymbol{K_I} := [K_{I_{11}}, K_{I_{12}}, \ldots, K_{I_{pq}}]$, $\boldsymbol{K_D} := [K_{D_{11}}, K_{D_{12}}, \ldots, K_{D_{pq}}]$, $\boldsymbol{N} := [N_{11}, N_{12}, \ldots, N_{pq}]$, $\boldsymbol{\zeta} := [\zeta_{11}, \zeta_{12}, \ldots, \zeta_{pq}]$, $\boldsymbol{\lambda} := [\lambda_{11}, \lambda_{12}, \ldots, \lambda_{pq}]$, $\boldsymbol{\alpha} := [\alpha_{11}, \alpha_{12}, \ldots, \alpha_{pq}]$, and $\boldsymbol{\sigma^2} := [\sigma_{11}^2, \sigma_{12}^2, \ldots, \sigma_{pq}^2]$. $w_{1j} \in \mathbb{R}$ $(j = 1, 2, \ldots, q)$ and $w_{2i} \in \mathbb{R}$ $(i = 1, 2, \ldots, p)$ further express the respective weightings of output and input as per determined by the system's designer. With the right side of equation (31) indicates both the tracking error term and the control input energy term, both values of w_{1j} and w_{2i} are confirmed based on undertaken preliminary experimentations, such that a well-balanced minimization between tracking error and control input energy is achieved.

Problem 3.1: Obtain $C_U(s)$ and $N_{MnHR}(\boldsymbol{e}(t), \Delta\boldsymbol{h}(t))$ of the MnHR-NEPID controller for MIMO gantry crane system such that the fitness function $J(\boldsymbol{K_P}, \boldsymbol{K_I}, \boldsymbol{K_D}, \boldsymbol{N}, \boldsymbol{\zeta}, \boldsymbol{\lambda}, \boldsymbol{\alpha}, \boldsymbol{\sigma^2})$, in accordance to the data $\boldsymbol{u}(t)$ and $\boldsymbol{y}(t)$, is minimized.

Application of RAMPA-based method with tunable CF *for tuning the MnHR-NEPID controller of MIMO gantry crane system*

Towards addressing the minimization of fitness function as per outlined in equation (31), this section is particularly dedicated to explain executed procedure for the optimization of MnHR-NEPID controller through the employment of RAMPA-based method with tunable *CF*. The process is initiated by mapping position vector of individual prey or agent $X_i \in \mathbb{R}^d$ from equation (1) to the design parameters of MnHR-NEPID controller, as follows

$$\boldsymbol{\psi} = \left[\boldsymbol{K_P}, \boldsymbol{K_I}, \boldsymbol{K_D}, \boldsymbol{N}, \boldsymbol{\zeta}, \boldsymbol{\lambda}, \boldsymbol{\alpha}, \boldsymbol{\sigma^2}\right] \in \mathbb{R}^d, \tag{32}$$

where each element of $\psi_j = 10^{X_{i,j}} (j = 1, 2, \ldots, d)$. The logarithmic scale has been especially adopted for the purpose of facilitating an accelerated process towards the attainment of design parameters.

With the fitness function f_i from equation (1) being concurrently mapped alongside the fitness function from equation (31) at $f_i = J(\boldsymbol{\psi})$, the designated fitness function of each agent is, therefore, written as $f_i\left(10^{X_{i,1}} \quad 10^{X_{i,2}} \quad \ldots \quad 10^{X_{i,d}}\right)$. Technicality wise, position of the agent $X_i(k)$ would be revised with operationalization of the proposed approach in conformity to the preys' location P_i by mean of minimizing value of the fitness function f_i. Dissimilar values of f_i are hereby generated by the updated $X_i(k)$ (from P_i) through paralleling both components of control input $\boldsymbol{u}(t)$ and error $\boldsymbol{e}(t)$. Ensuing

ranking of each produced f_i, f_i with the best value would be subsequently recorded, whilst having its respective best position vector being registered as $X_i^{'}(k)$ of matrix E. Required procedure for updating the position vector of each agent $X_i(k)$ has been systematically detailed in **Algorithm 1**, in accordance to the tuning operation of MnHR-NEPID controller. Such duplex coordination between the proposed RAMPA-based method with tunable *CF* and MnHR-NEPID controller of the MIMO gantry crane system is repetitively operationalized prior reaching the maximum iteration. The methodical procedure towards optimization of the data-driven MnHR-NEPID controller is essentially summarized by:

Step 1: The mapping of $f_i = J(\boldsymbol{\psi})$ and $X_{i,j} = log\psi_j (j = 1, 2, \ldots, d)$ is established. Following this, *UB, LB,* $k_{max}, n, d, Q, FADs$, and β are determined.

Step 2: Updating procedure of the RAMPA-based method with tunable *CF* from **Algorithm 1** is operationalized.

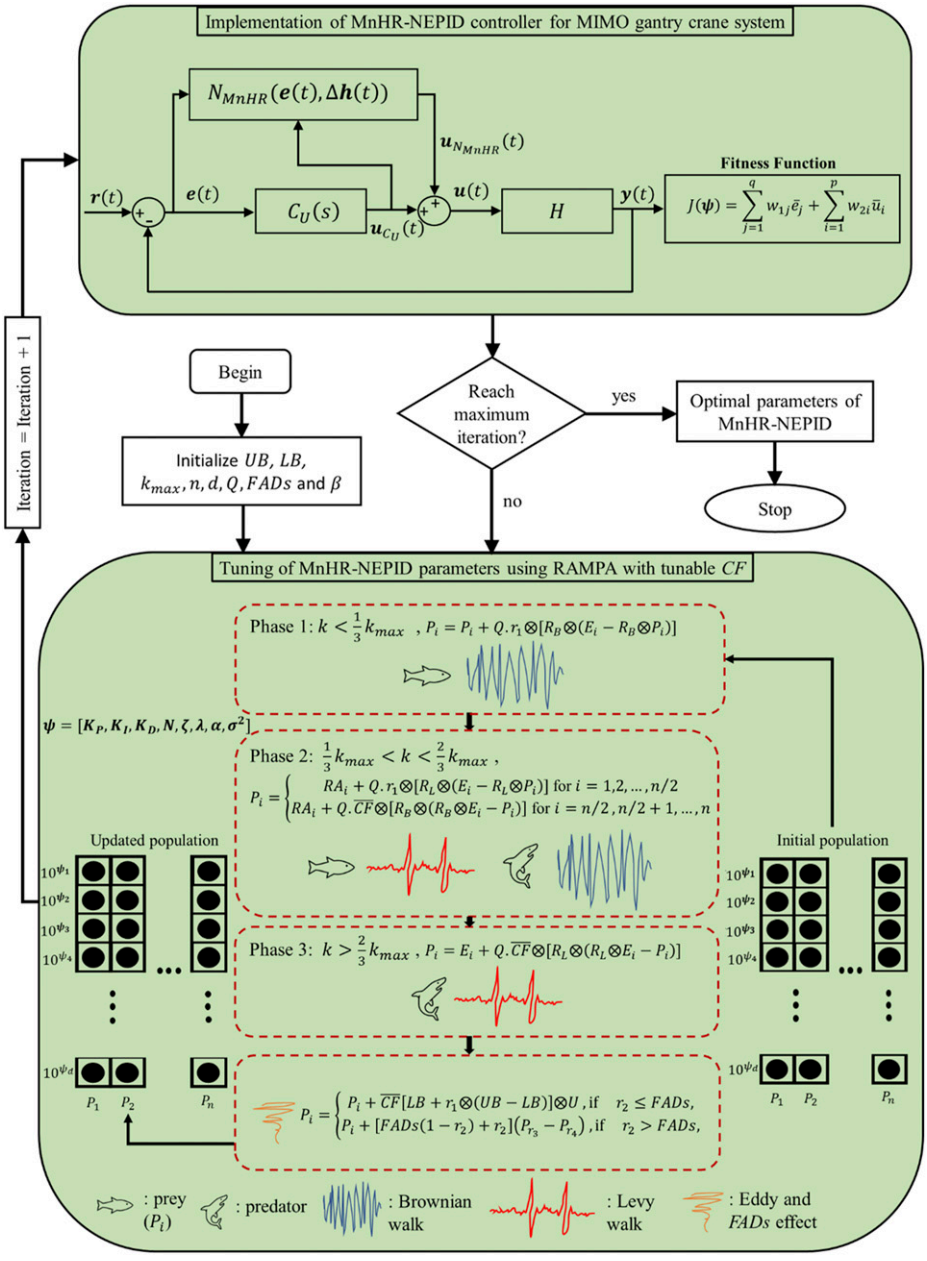

Figure 5. Block diagram of RAMPA-based method with tunable CF implementation for MnHR-NEPID controller of MIMO gantry crane system.

Step 3: Upon reaching the maximum iteration k_{max}, optimal design parameters $X_i^{'}$ would be obtained from elite matrix E. The acquired optimal design parameters are further implemented to $C_U(s)$ and $N_{MnHR}(\boldsymbol{e}(t), \Delta\boldsymbol{h}(t))$ as solution for the MnHR-NEPID controller in Figure 4.

Remarks 3.1: The tuning method for MnHR-NEPID controller for the current study especially implements a data-driven or model-free approach. The examined MIMO gantry crane system is, therefore, perceived as a "black box" model, with exclusive parameters of the MnHR-NEPID controller as employed for the system being fine-tuned based entirely on obtained information concerning the given input and output data at the absence of an established plant model.

A comprehensive flow diagram encompassing tuning approach as employed for the MnHR-NEPID controller using RAMPA-based method with tunable *CF* is entirely outlined in Figure 5. As observed, two key blocks have been detailed, enclosing both the implementation of the MnHR-NEPID controller for MIMO gantry crane system and the operationalization of RAMPA-based method with tunable *CF*. The first block sets towards attaining the minimal fitness function $J(\boldsymbol{\psi})$ by exploiting on the previously determined input $\boldsymbol{u}(t)$ and output $\boldsymbol{y}(t)$. Further retrieved from P_i, **Algorithm 1** is subsequently performed upon mapping f_i to $J(\boldsymbol{\psi})$ within the second block in seek of acquiring the updated design parameter of individual prey X_i. Updated design parameter would then be adopted to the first block by definition of $\psi_j = 10^{X_{i,j}} (j = 1, 2, \ldots, d)$. Such reciprocated circulation between both blocks is repetitively executed pending maximum iterations in realizing the optimal design parameter $X_i^{'}$.

Implementation and results

The current section discusses appraised performance of the MIMO gantry crane control system with employment of MnHR-NEPID controller fine-tuned using the proposed RAMPA-based method with tunable *CF*. Comparison is fundamentally made between effectiveness of the proposed approach, the conventional MPA-based method, and other existing metaheuristic-based algorithms, viz. PSO,[48] GWO,[49] MFO,[50] MVO,[51] SCA,[52] SSA,[53] SMA,[54] and FDA.[55] Recorded outcomes from the introduced RAMPA-based method with tunable *CF* are further evaluated against the formerly published ASED-based method.[35] Performances of the examined algorithms are essentially assessed by virtue of the following criteria

1. Convergence curves of average fitness function (out of 25 trials) as generated from RAMPA-based method with tunable *CF* and the conventional MPA, PSO, GWO, MFO, MVO, SCA, SSA, SMA, and FDA-based methods are contrasted. Inspection is especially made on the algorithms' capacities to minimize their generated fitness function.
2. Fitness function $J(\boldsymbol{K_P}, \boldsymbol{K_I}, \boldsymbol{K_D}, \boldsymbol{N}, \boldsymbol{\zeta}, \boldsymbol{\lambda}, \boldsymbol{\alpha}, \boldsymbol{\sigma^2})$ from equation (31), the total norm of error $\sum_{j=1}^{q} \overline{e}_j$, and the total norm of input $\sum_{i=1}^{p} \overline{u}_i$ as acquired through 25 independent trials with reference to the mean, best, worst, and standard deviation (std.) are statistically evaluated. As per mentioned, comparison is undertaken between the obtained statistical analysis from RAMPA-based method with tunable *CF*, the conventional MPA-based method, and the formerly stated algorithms.
3. Non-parametric statistical analysis by employment of the Wilcoxon's rank test is pursued to engage the statistical dissimilarity between examined algorithms at a significance level of 5%. Statistical test is essentially proceeded between a pair of distinct algorithms by primarily contrasting their respective mean values to observe the significance level based on its $p - value$. Significant divergence is established between simulated outcomes and efficiency of respective algorithms in the case where $p - value < 0.05$. On the contrary, divergence between simulated outcomes of respective algorithms is deemed insignificant in the case where $p - value > 0.05$. Additionally, the box plot is considered to evaluate the precision of the algorithms.
4. Time responses analysis of MIMO gantry crane system as acquired through employment of the proposed RAMPA-based method with tunable *CF* and the preceding ASED-based approach[35] are appraised with respect to its trolley displacement $y_1(t)$, length of the rope $y_2(t)$, sway angle of the payload $y_3(t)$, trolley force $u_1(t)$, and hoist force $u_2(t)$.
5. Robustness of the MnHR-NEPID controller as optimized using the RAMPA-based method with tunable *CF* and the ASED-based method[35] is assessed with introduction of external disturbance to the MIMO gantry crane system.

Attempted simulations for the current study were performed based on MATLAB/Simulink R2020a using a personal computer equipped with the specification of Microsoft Window 10, 8 GB RAM and Intel Core i7-6700 Processor (3.41 GHz). The MnHR-NEPID control system as outlined in Figure 4 has been explicitly adopted for the control of MIMO gantry crane system in Figure 3 at a total number of outputs $q = 3$ and inputs $p = 2$. Respective inputs and outputs of the

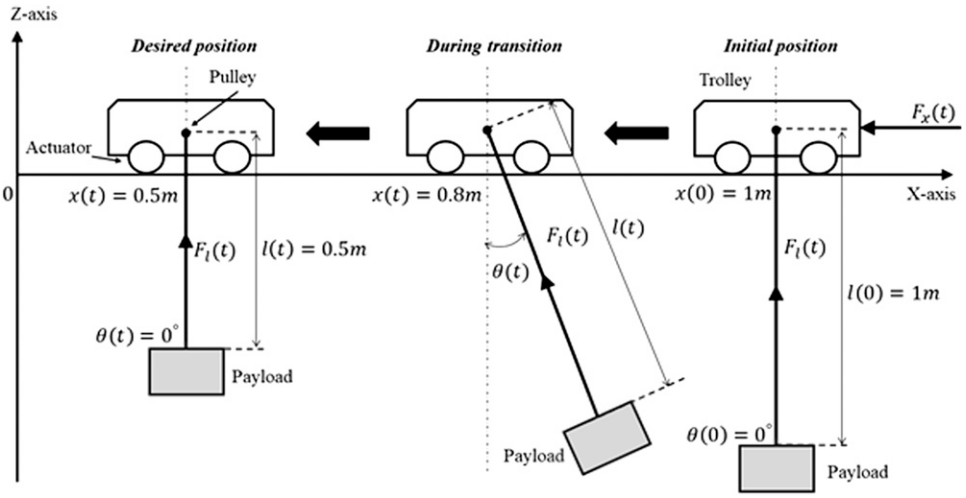

Figure 6. The trolley's movement and the rope's length adjustment to the desired position.

studied system are further signified by $u_1(t) = F_x(t), u_2(t) = F_l(t), y_1(t) = x(t), y_2(t) = l(t)$ and $y_3(t) = \theta(t)$. As opposed to the previous work in ref. 35 which considered a trolley displacement from 1 m to the origin and a rope's length adjustment from 1 m to 0.2 m, a shorter trolley displacement and adjustment of the rope's length is accounted for the current research at a reduced simulation time to minimize the required computation duration for the system's tuning. With this in mind, the desired trolley's position, length of the rope, and sway angle are then considered as

$$\boldsymbol{r}(t)_{3\times1} = [\,0.5 \quad 0.5 \quad 0\,]^T \forall t, \tag{33}$$

with initial position of the trolley, length of the rope, and sway angle of the payload being independently given at $x(0) = 1$, $l(0) = 1$, and $\theta(0) = 0$. Heightened clarification is further expressed through Figure 6 which comprehensively illustrates the trolley's movement and the rope's length adjustment approaching their desired positions. As observed, initial position of the trolley has been determined at 1 m from the origin, with initial length of the rope being conjointly determined at 1 m. Thereafter, the trolley's actuator is maneuvered forwarding the left sided direction approaching its desired position of 0.5 m. In the meantime, adjustment is also undertaken by the installed pulley on the rope towards the desired length of 0.5 m. With both swaying and oscillation of the involved payload being discernable throughout the trolley's maneuver between both locations; this study, nonetheless, aims in transferring the payload to its desired position at a minimal sway angle.

MnHR-NEPID controller for the MIMO gantry crane system from Figure 4 has been fundamentally considered as

$$C_U(s)_{2\times3} = \begin{bmatrix} C_{11}(s) & 0 & C_{13}(s) \\ 0 & C_{22}(s) & 0 \end{bmatrix} \tag{34}$$

and

$$N_{MnHR}(\boldsymbol{e}(t), \Delta\boldsymbol{h}(t))_{2\times3} = \begin{bmatrix} Y_{V_{11}} & 0 & Y_{V_{13}} \\ 0 & Y_{V_{22}} & 0 \end{bmatrix}. \tag{35}$$

With reference to equation (20), four design parameters for each $C_{ij}(s)$ controller are hereby accounted. Likewise, four other design parameters as stated in equations (22)–(26) are alternatively considered for each of the $N_{MnHR}(\boldsymbol{e}(t), \Delta\boldsymbol{h}(t))$ controller. Corresponding to $\boldsymbol{\psi} = [\boldsymbol{K_P}, \boldsymbol{K_I}, \boldsymbol{K_D}, \boldsymbol{N}, \boldsymbol{\zeta}, \boldsymbol{\lambda}, \boldsymbol{\alpha}, \boldsymbol{\sigma^2}] \in \mathbb{R}^{24}$, a total number of 24 design parameters are then contemplated for the employed MnHR-NEPID controller. Initial position of each design parameter has further been randomly assigned in accordance to the previous discussion in Section 2.1 to enable increased possibility among agents for the exploration of search domains within their predetermined boundary. Implementation of the proposed RAMPA-based method with tunable *CF*, thus, bypassed the time-consuming complicatedness of tedious preliminary investigations as operationalized in ref. 35 towards determining feasible initial design parameters of the chosen controller. Objectively, the fitness function in equation (31) is minimized by obtaining $\boldsymbol{\psi} \in \mathbb{R}^{24}$, with the weighting coefficients being set at $w_{11} = 200$, $w_{12} = 400$, $w_{13} = 200$, $w_{21} = 1$, and $w_{22} = 1$ to reflect the circumstance of Ref.[35]. The error threshold T_h as included in equation (25) is similarly identified to such condition at a value of 0.05. Nevertheless, the simulation time in ref. 35 has been halved for the current

Table 1. Coefficients of PSO, GWO, MFO, MVO, SCA, SSA, SMA, and FDA.

Algorithm	Coefficients
PSO	$W_{max} = 0.9, W_{min} = 0.2, c_1 = 2, c_2 = 2, V_{max} = 6$
GWO	$a = 2^*\left(1 - \left(\frac{k}{k_{max}}\right)\right)$
MFO	$r = -1 + k^*\left(\frac{-1}{k_{max}}\right)$
MVO	$WEP_{min} = 0.2, WEP_{max} = 1, p = 6$
SCA	$r_1 = 2^*\left(1 - \left(\frac{k}{k_{max}}\right)\right)$
SSA	$c_1 = 2e^{-\left(\frac{4k}{k_{max}}\right)^2}$
SMA	$a = arctanh\left(-\left(\frac{k}{k_{max}}\right) + 1\right)$
	$z = 0.03$
FDA	$\beta = 1$

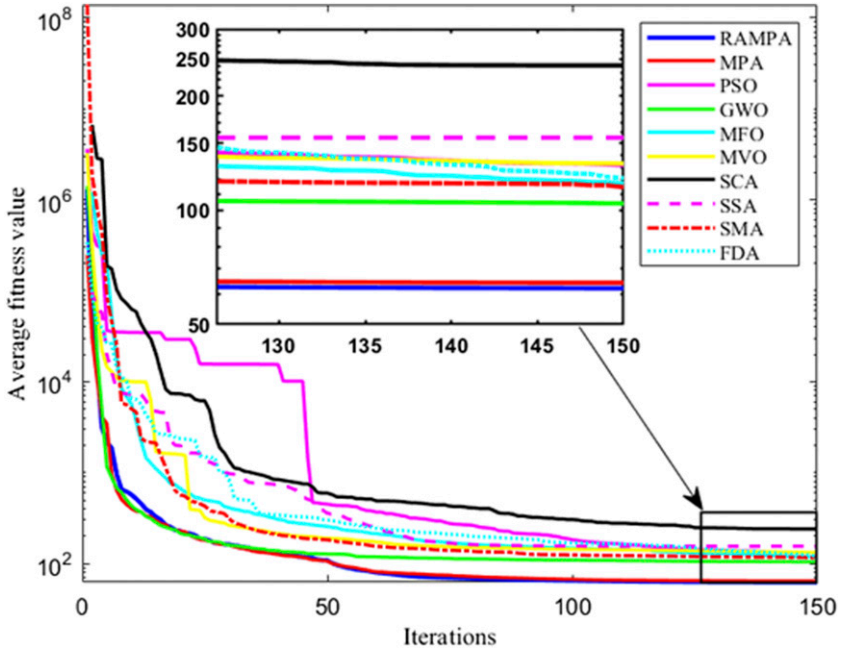

Figure 7. Convergence curves of the average fitness function from 25 trials.

study to a designated interval of $t_f = 10$ s. In view of the optimization related settings, both the upper bound and lower bound for each design parameter have been primarily determined at the values of $UB = 2.5$ and $LB = -2.5$. The maximum number of iterations and the number of agents are further determined at $k_{max} = 150$ and $n = 20$, respectively. Such settings essentially contributed a total of 3000 number of function evaluations (NFE). Several preliminary investigations subsequently established the coefficient for RAMPA-based method with tunable CF at a value of $\beta = 0.8$. Default coefficients of the MPA-based method are ultimately maintained succeeding implementation of the RAMPA-based method with tunable CF at $Q = 0.5$ and $FADs = 0.2$. With each statistical element in place, 25 independent trials under the identical set of coefficients were simulated to appraise the robustness of RAMPA-based method with tunable CF against the randomization effect. Meanwhile, the coefficients of other existing algorithms as examined in this paper, comprising the PSO, GWO, MFO, MVO, SCA, SSA, SMA, and FDA-based methods, are thoroughly tabulated in Table 1.

Table 2. The statistical performance value of fitness function, total of norm error, total of norm input, and its corresponding average CPU time.

Algorithm		RAMPA	MPA	PSO[48]	GWO[49]	MFO[50]	MVO[51]	SCA[52]	SSA[53]	SMA[54]	FDA[55]
J	**Mean**	**62.2543**	64.4061	131.4303	104.1759	117.4901	132.6459	240.3776	78.7033	114.9545	121.37
	Best	**59.299**	59.9417	66.8138	68.2634	66.6816	60.22	96.3742	65.2359	61.4987	70.02
	Worst	**71.4381**	72.1807	323.2	312.6823	268.3419	389.12	504.6742	270.8157	418.7346	267.84
	Std	**3.0196**	3.7814	69.8926	62.8759	54.1885	106.6542	123.5538	78.7033	80.9156	52.11
$\sum_{j=1}^{3} \bar{e}_j$	**Mean**	**0.1949**	0.2027	0.4744	0.3675	0.4072	0.4879	0.7769	0.5702	0.4044	0.37
	Best	**0.1802**	0.1856	0.1999	0.2161	0.2182	0.1855	0.2827	0.1970	0.1875	0.22
	Worst	**0.2345**	0.2444	1.4679	1.3984	0.9885	1.4396	2.0263	1.2519	1.6241	1.02
	Std	**0.0132**	0.0161	0.3304	0.3029	0.2073	0.4312	0.4957	0.3687	0.3302	0.17
$\sum_{i=1}^{2} \bar{u}_i$	**Mean**	**10.5743**	11.032	11.3402	11.2301	12.7837	11.6458	31.366	14.1230	11.0013	18.63
	Best	7.7011	8.8831	1.2869	1.013	2.5483	4.9	**0.7258**	3.3682	2.6191	4.23
	Worst	**12.8519**	14.4353	27.3371	17.4691	85.9382	31.6376	114.6787	92.5601	25.4499	72.14
	Std	**1.112**	1.3651	6.9365	3.9105	16.0989	4.8319	30.3937	16.8364	5.0618	17.06
Average CPU Time(s)	**Mean**	3.27E + 03	3130.5	1.58E + 03	1.61E + 03	1.58E + 03	1.64E + 03	**1.56E + 03**	1572.5883	1.60E + 03	1.60E + 03

Table 3. Wilcoxon's rank test of the fitness function between the RAMPA-based method with tunable CF and other based methods.

	RAMPA with tunable *CF* Versus								
Algorithm	**MPA**	**PSO[48]**	**GWO[49]**	**MFO[50]**	**MVO[51]**	**SCA[52]**	**SSA[53]**	**SMA[54]**	**FDA[55]**
p* − *value	0.0189	2.8980E−9	2.8980E − 9	2.2857E − 9	2.7218E − 7	1.4157E − 9	2.5742E − 9	1.3090E − 7	1.596E − 9
S^+	223	325	325	325	281	325	325	306	325
S^-	102	0	0	0	44	0	0	19	0

Remarks 4.1: The maximum number of iterations, the upper bounds, the lower bounds, and the number of agents are identically set for RAMPA-based method with tunable *CF* and each examined-based method to ensure comparable performance assessments.

The convergence curves for average fitness function as generated from 25 trials by the RAMPA-based method with tunable *CF*, as well as the conventional MPA, PSO, GWO, MFO, MVO, SCA, SSA, SMA, and FDA-based methods have been comprehensively plotted in Figure 7. Recorded response through employment of the proposed RAMPA-based method with tunable *CF* is particularly denoted by a thicker, blue-colored line alongside other thinner, colored lines that represent the obtained responses from other examined algorithms. Further observed through the magnified plot as illustrated within said figure, the proposed algorithm has demonstrated excellence in minimizing the fitness function of equation (31) approaching final iteration of the simulation over the performances of other peripheral-based methods. Its proficiency in minimizing the fitness function has, nonetheless, been firmly justified. However, statistical performances of the examined algorithms in terms of the fitness function J, total of norm error $\sum_{j=1}^{3} \bar{e}_j$, total of norm input $\sum_{i=1}^{2} \bar{u}_i$, and average CPU time are further registered and exclusively depicted in Table 2. Highlighted in bold, RAMPA-based method with tunable *CF* has dominated majority of the assessed domains for generating comparatively superior results against its predecessors. Such is on the exception of the average CPU time, with SCA-based method committing the shortest duration due to its relatively simpler operational principle,[52] as compared to the three segregated phases and accounted environmental issues within execution of the MPA-based method. With adherence to the explanation in Section 2.2, supplementary efforts as attempted by the proposed algorithm towards computation of random average would contribute a longer average CPU time. In the case where a supercomputer is employed to overcome such shortfall in computation time, obtained verdict from the aspects of fitness function, total of norm error, and total of norm input have, thus, elevated RAMPA-based method with tunable *CF* as a noteworthy optimization approach.

On a similar note, a non-parametric statistical test by employment of the Wilcoxon's rank test at a significance level of 5% was implemented to appraise the statistical difference in fitness function among each examined-based method.

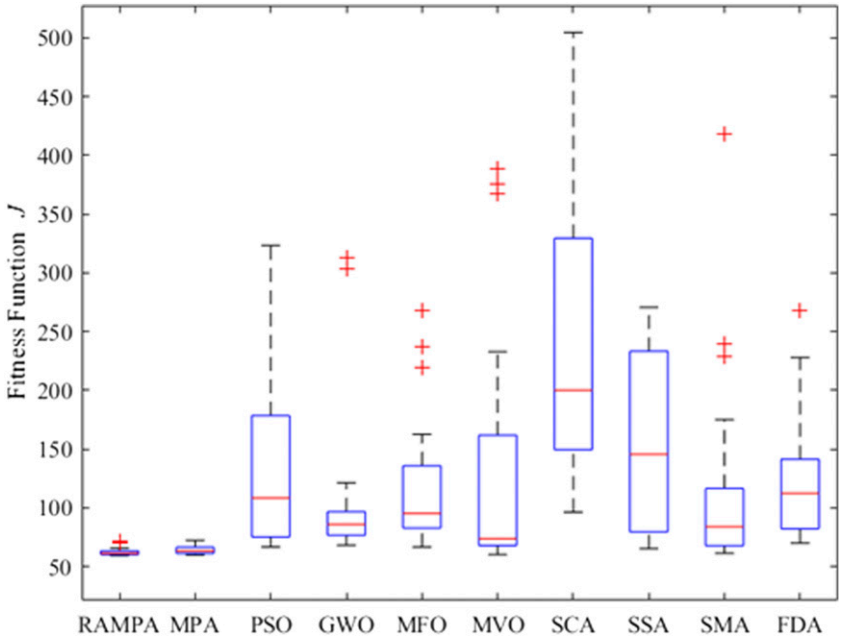

Figure 8. Box plot of the fitness function produced by different algorithms from 25 trials.

Obtained results from the Wilcoxon's rank test for pair-wise between the RAMPA-based method with tunable *CF* and the other contrasted-based methods are then entirely tabulated in Table 3. In view of the recorded sum of ranks, superior performance has been comparatively demonstrated by the proposed algorithm against the rivaling algorithms when $\mathbf{S}^{+}$, with the yielding of contradictory outcome when $\mathbf{S}^{-}$.[56] Comprehensive registration of $\mathbf{S}^{+}$ by RAMPA-based method with tunable *CF* against its sparing contenders have further signified evident disparities between the proposed algorithm and its predecessors. Recorded $p-values$ between the proposed algorithm and the other examined based methods of less than 0.05 have concurrently confirmed statistical significance of the former's comparably robust optimization competency. Moreover, developed box plots for the fitness function of each examined algorithm have been graphically presented in Figure 8. Likewise, the smallest interquartile range as produced by the proposed RAMPA-based method with tunable *CF* has justified its performance excellence with respect to its fitness function. A heightened degree of consistency as exhibited by the proposed algorithm, thus, substantiated its competitive performance precision.

Criteria are subsequently set on the evaluation of time responses with the purpose of accentuating both the proposed algorithm's optimization dominance and proficiency. On this account, observation is especially made on the rise time T_r, the settling time T_s, percentage overshoot $\%OS$ of trolley displacement $y_1(t)$, length of the rope $y_2(t)$, maximum sway angle of the payload $y_3(t)$, as well as the maximum inputs of both trolley force $u_1(t)$ and hoist force $u_2(t)$; to assess the accuracy of MnHR-NEPID controller in controlling a MIMO gantry crane system through the employment of dissimilar metaheuristic-based methods. The aforementioned settling time is hereby understood as duration the system would require to achieve 2% of the predetermined final response value, whilst rise time being duration the system would require to progress between 10% and 90% of said final response value. Comparison has been exclusively proceeded between the proposed algorithm and the ASED based method as formerly introduced in ref. 35. Notably, contemporary fine-tuning of design parameters for MnHR-NEPID controller within the current study has been operationalized in advertence to simulated nature of the previously investigated ASED-based method.[35] In this regard, initial values of the design parameters, coefficients of the ASED based method, and weighting coefficient from ref. 35 are thoroughly retained towards controlling the MIMO gantry crane system.

Optimal design parameters of the MnHR-NEPID controller based on both the proposed RAMPA-based method with tunable *CF* and the ASED-based method, alongside the respective fitness function of each algorithm, have then been tabulated in Table 4. As such, the optimal control parameters are especially decided apropos ideal of the lowest fitness function as generated via 25 independent trials prior simulated implementations for the controlling of MIMO gantry crane system to appraise the time responses as acquired through a number of output responses. As observed

Table 4. Optimal MnHR-NEPID controller parameters with corresponding fitness function obtained by RAMPA and ASED-based methods for MIMO gantry crane system.

		RAMPA		ASED[35]	
ψ	MnHR-NEPID	X_i'	$10^{X_i'}$	X_i'	$10^{X_i'}$
ψ_1	$K_{P_{11}}$	0.624128	4.208506	0.412453	2.584952
ψ_2	$K_{I_{11}}$	2.300254	199.6431	1.922952	83.74372
ψ_3	$K_{D_{11}}$	−0.19479	0.638567	0.122947	1.327233
ψ_4	N_{11}	0.874059	7.482708	1.158438	14.40249
ψ_5	ζ_{11}	−1.18688	0.065032	−1.21144	0.061455
ψ_6	λ_{11}	−1.73407	0.018447	−2.21508	0.006094
ψ_7	α_{11}	−1.33116	0.046648	−0.74954	0.178018
ψ_8	σ_{11}^2	0.866984	7.361804	1.564149	36.65633
ψ_9	$K_{P_{13}}$	1.427022	26.73145	1.084276	12.1416
ψ_{10}	$K_{I_{13}}$	−0.11684	0.764124	−0.46581	0.342128
ψ_{11}	$K_{D_{13}}$	−0.85244	0.140462	−0.46397	0.343583
ψ_{12}	N_{13}	0.094668	1.243563	0.462779	2.902543
ψ_{13}	ζ_{13}	1.004612	10.10675	0.622977	4.197364
ψ_{14}	λ_{13}	0.095831	1.246899	0.981306	9.578697
ψ_{15}	α_{13}	−0.66333	0.217106	0.335253	2.16398
ψ_{16}	σ_{13}^2	0.179427	1.511566	1.196119	15.70794
ψ_{17}	$K_{P_{22}}$	0.819675	6.601997	0.793758	6.219541
ψ_{18}	$K_{I_{22}}$	0.202942	1.595667	0.248673	1.772853
ψ_{19}	$K_{D_{22}}$	0.061326	1.151664	0.352263	2.250417
ψ_{20}	N_{22}	−0.1493	0.709081	0.543821	3.498013
ψ_{21}	ζ_{22}	−1.08102	0.082982	0.004553	1.01054
ψ_{22}	λ_{22}	0.0412	1.099513	−3.08616	0.00082
ψ_{23}	α_{22}	−1.08359	0.082491	−3.11668	0.000764
ψ_{24}	σ_{22}^2	−1.69782	0.020053	−2.82184	0.001507
J		**59.299**		59.7851	

within the detailed table, a marginally diminished fitness function is recorded from the parameters of the proposed algorithm at a value of 59.299 against a value of 59.7851 from the ASED-based method. Although the ASED-based method has the advantage of choosing the initial design parameters that are quite closed with the optimal design parameters, the RAMPA-based method with tunable *CF* can still produce better fitness function.

Following this, the output responses alongside their magnified versions of $y_1(t)$, $y_2(t)$, and $y_3(t)$ have been separately outlined through Figures 9–11; with the control input responses $u_1(t)$ and $u_2(t)$ alongside their magnified versions being individually presented through Figures 12 and 13. Coinciding with the previous criterion, comparison is especially proceeded between both the proposed RAMPA-based method with tunable *CF* and the ASED-based method.[35] Nevertheless, the proposed algorithm has fundamentally exerted dominating output responses in terms of trolley displacement $y_1(t)$ for generating a relatively shorter settling time of T_s = 2.42 s, against the competing ASED-based method with a settling time of T_s = 2.8 s. However, the latter approach has demonstrated outshining results for both the recorded rise time T_r and the percentage overshoot $\%OS$ at the respective outcomes of T_r = 1.037 s and 5.9%, as compared to the registered results of T_r = 1.06 s and 7.9% from the proposed algorithm. With this being said, reported discrepancies in performance of the proposed algorithm do not compromise its exceptional applicability and output performance within a MIMO gantry crane system.

Forwarded with response evaluation of the rope's length $y_2(t)$, a shorter settling time has, yet again, been recorded by the RAMPA-based method with tunable *CF* at a value of T_s = 1.19 s, against the result of T_s = 1.668 s from the ASED-based method. Such excellence is similarly identified within the aspect of percentage overshoot $\%OS$, in which the 5.74% as produced by the ASED-based method is being considerably outperformed by the proposed algorithm with a percentage of 3.76%. In spite of a marginally superior response rate as demonstrated by the ASED-based method over the proposed RAMPA-based method with tunable *CF* amidst the transient state following their respective performances of T_r = 0.445 s

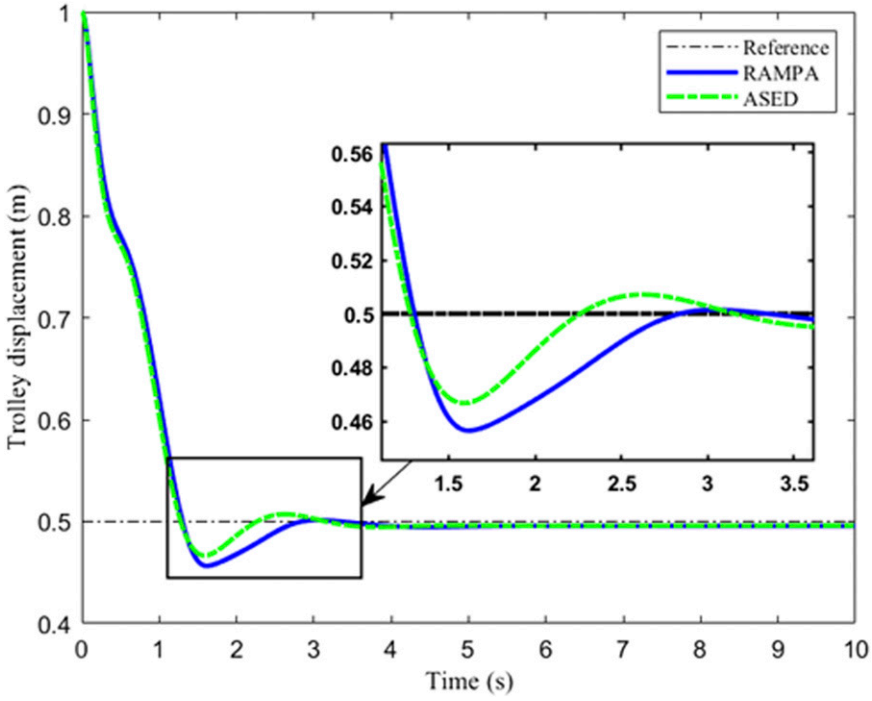

Figure 9. Trolley displacement $y_1(t)$ responses.

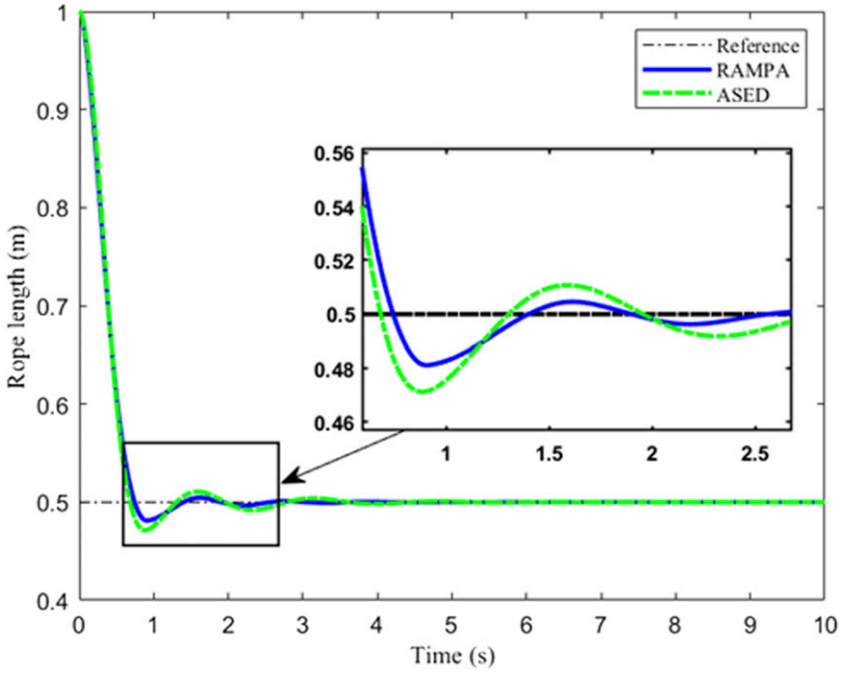

Figure 10. Rope length $y_2(t)$ responses.

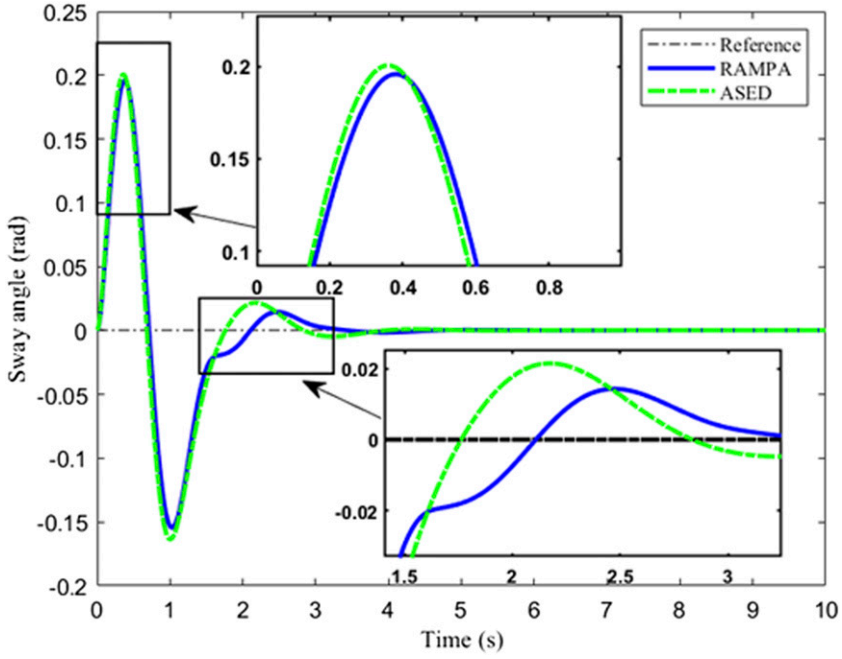

Figure 11. Sway angle $y_3(t)$ responses.

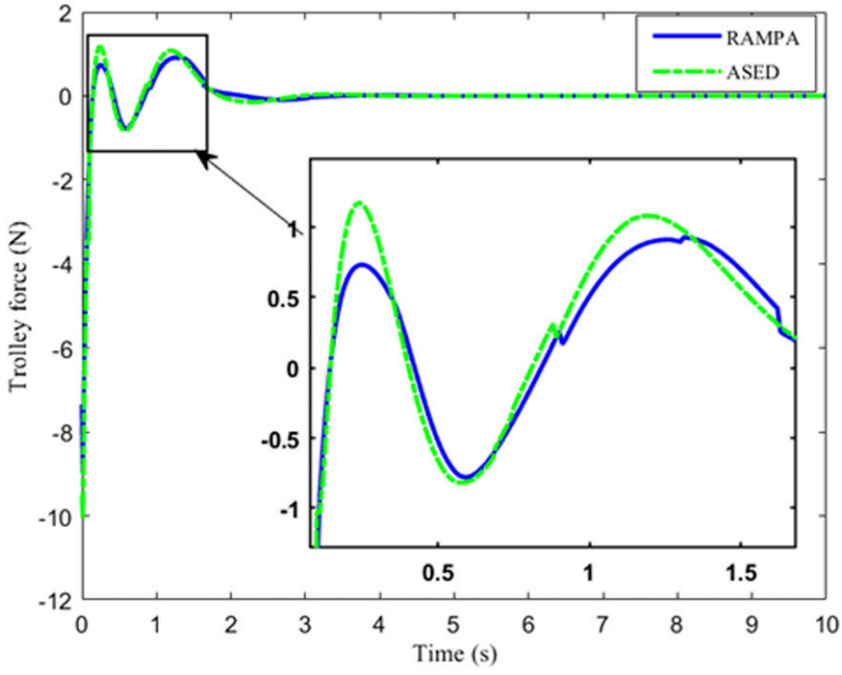

Figure 12. The trolley force $u_1(t)$ responses.

and $T_r = 0.49$; noticeable excellence as exhibited by the proposed algorithm in both aspects of settling time and percentage overshoot have undeniably conformed its proficiency as the better optimization approach for rope length performance criteria.

Further outlined in Figure 11, attention is consequently relocated to the controllers' responses to oscillations in the system's payload based on the registered sway angles $y_3(t)$ throughout its transition. Herewith, the proposed

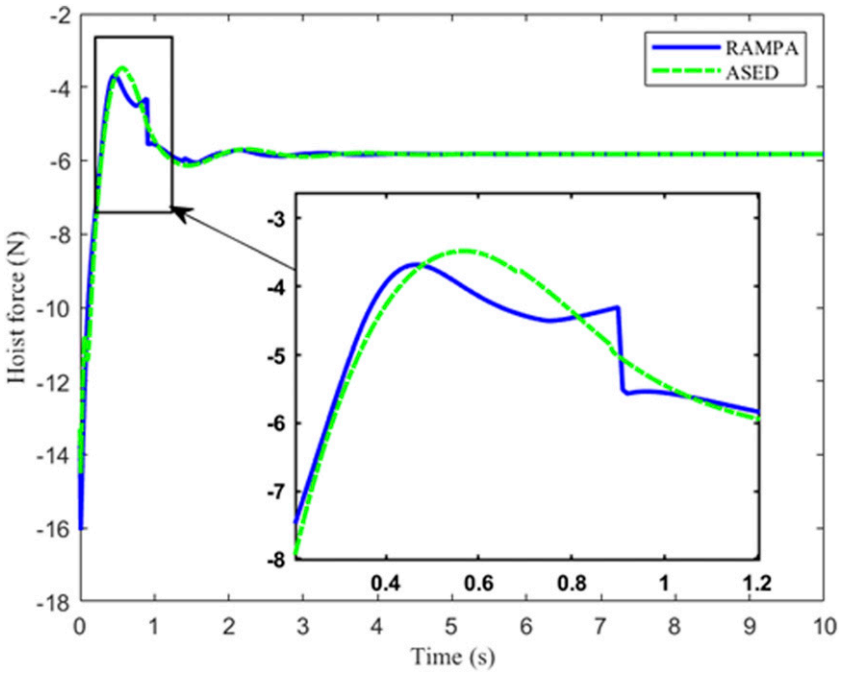

Figure 13. The hoist force $u_2(t)$ responses.

Table 5. The results of time responses analysis of the MIMO gantry crane system.

Response	Performance parameters	RAMPA	ASED[35]
$y_1(t)$	Rise time, T_r (s)	1.06	**1.037**
	Settling time, T_s (s)	**2.42**	2.8
	Percentage overshoot, $\%OS$ (%)	7.9	**5.9**
$y_2(t)$	Rise time, T_r (s)	0.49	**0.445**
	Settling time, T_s (s)	**1.19**	1.668
	Percentage overshoot, $\%OS$ (%)	**3.76**	5.74
$y_3(t)$	Maximum sway angle (radian)	**0.1958**	0.2006
	Settling time, T_s (s)	**1.63**	2.27
$u_1(t)$	Maximum input (N)	**0.9261**	1.172
	Minimum input (N)	**−8.978**	−10.05
$u_2(t)$	Maximum input (N)	−3.681	**−3.479**
	Minimum input (N)	−16.06	**−14.51**

RAMPA-based method with tunable *CF* has similarly generated an overshadowing response to the payload's oscillations through its relatively smaller maximum sway angle of 0.1958 radian and a shorter settling time of T_s = 1.63 s, as compared to the recorded maximum sway angle of 0.2006 radian and settling time of T_s = 2.27 s from the ASED-based method. Alternatively, results acquired for both the trolley force $u_1(t)$ and the hoist force $u_2(t)$ as, respectively, outlined in Figures 12 and 13 have showcased competitive outcomes between the proposed algorithm and its compared algorithm counterpart. Such has been utmost apparent following a marginally greater trolley force $u_1(t)$ as generated by the ASED-based method between the range of ≈ - 10.05 N and 1.172 N, over the lower control input of RAMPA-based method with tunable *CF* that falls between the range of ≈ −8.978 N and 0.9261 N. On the contrary, a relatively smaller hoist force $u_2(t)$ was propelled by the ASED-based method between the range of ≈ −14.51 N to −3.479 N, as compared to the proposed algorithm with a greater control input that falls between the range of ≈ −16.06 N and −3.681 N. Whilst a higher hoist force was yielded by the proposed algorithm, a shorter settling time corresponding to encountered transformation in the rope's length $y_2(t)$ as per previously reported

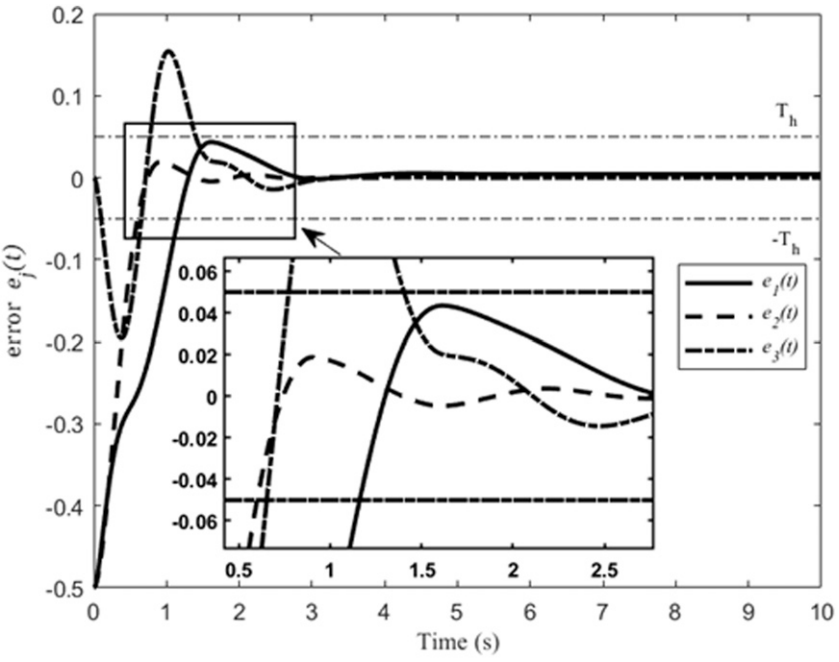

Figure 14. The error responses for the MIMO gantry crane system by using RAMPA-based method with tunable CF.

through Figure 10 has, nonetheless, reassured the approach's superior compatibility in regulating and simultaneously achieving the appropriated length of the rope within a MIMO gantry crane system. In view of an enhanced positional precision and a diminished sway angle on the system's payload, comprehensive analyses undertaken towards recorded time responses have, therefore, advocated the proposed RAMPA-based method with tunable *CF* as an excellent approach for the optimization of MnHR-NEPID controller. Collective findings from such appraisals are further summarized and tabulated in Table 5.

Emphasis is subsequently allocated to the analyzing of interrelationship between both responses of error and switching mechanism. Herewith, control variable error responses for trolley displacement, length of the rope, and sway angle ($e_1(t)$, $e_2(t)$, and $e_3(t)$) as generated by RAMPA-based method with tunable *CF* have been cumulatively demonstrated in Figure 14. Magnified results of switching mechanisms η_1, η_2, and η_3 as previously expressed in equation (25) for the operationalization of multiple nodes are further illustrated through Figures 15(a)–(c). In particular, regulation of the involved switching mechanisms would solely rely on the control variable error of $-T_h > e_j(t) > T_h$ in accordance to the normalized Gaussian function as formerly stated in equation (26). Observed through Figure 14, multiple nodes were activated ensuing a comparatively higher control variable error response that surpassed the error threshold of $T_h = \pm 0.05$ yielded between respective simulated intervals of 0–1.1 s, 0–0.6 s, and 0–1.4 s for the individual factors of $e_1(t)$, $e_2(t)$, and $e_3(t)$. Pinpointed via the illustrated data tips, the magnified results of switching mechanism η_1 as presented in Figure 15(a) then regulated exponentially between the values of 0 to 1 following transformation in the control variable error from ± 0.05 to ± 4.67. Similar circumstance is encountered for the magnified results of switching mechanism η_2 as presented in Figure 15(b) with its value shifted from 0 to 1 ensuing change in the control variable error from ± 0.05 to ± 1.28. On the same note, magnified results of switching mechanism η_3 as showcased in Figure 15(c) have demonstrated a pointier curve in normalized Gaussian function against its η_1 and η_2 counterparts, whilst shifted its value from 0 to 1 upon experiencing a change in the control variable error from $\pm$ 0.05 to $\pm$ 0.64. Conversely, the control variable error responses $e_1(t)$, $e_2(t)$, and $e_3(t)$ in Figure 14 for time intervals 1.16–10 s, 0.6–10 s, and 1.4–10 s, respectively, produce less control variable error than the threshold $T_h = \pm 0.05$. In this situation, the switching mechanisms became 0 as illustrated in Figure 15(a)–(c). Therefore, instead of using multiple nodes hormone regulation, the single-node hormone regulation of the standard NEPID would be implemented. Thus, the total interactions of the switching mechanism for MnHR-NEPID controller would reduce the high control variable error that exceed the error threshold in order to produce better control accuracy.

In consideration of the algorithms' applicability facing circumstance of uncertainties, performances of MnHR-NEPID controller following implementations of the proposed RAMPA with tunable *CF* and the compared ASED-based method

have been assessed under the situations of unexpected disturbance. In this case, simulation was performed on the examined MnHR-NEPID–based method through introduction of disturbance $\boldsymbol{d}(t) = \begin{bmatrix} 0 & 0 & d_{y_3}(t) \end{bmatrix}^T$ to the MIMO gantry crane system. Succeeding settings of the disruptive signals in accordance to the illustration in Figure 16, external disturbance was applied to the sway angle $y_3(t)$ at a given equation as per follows

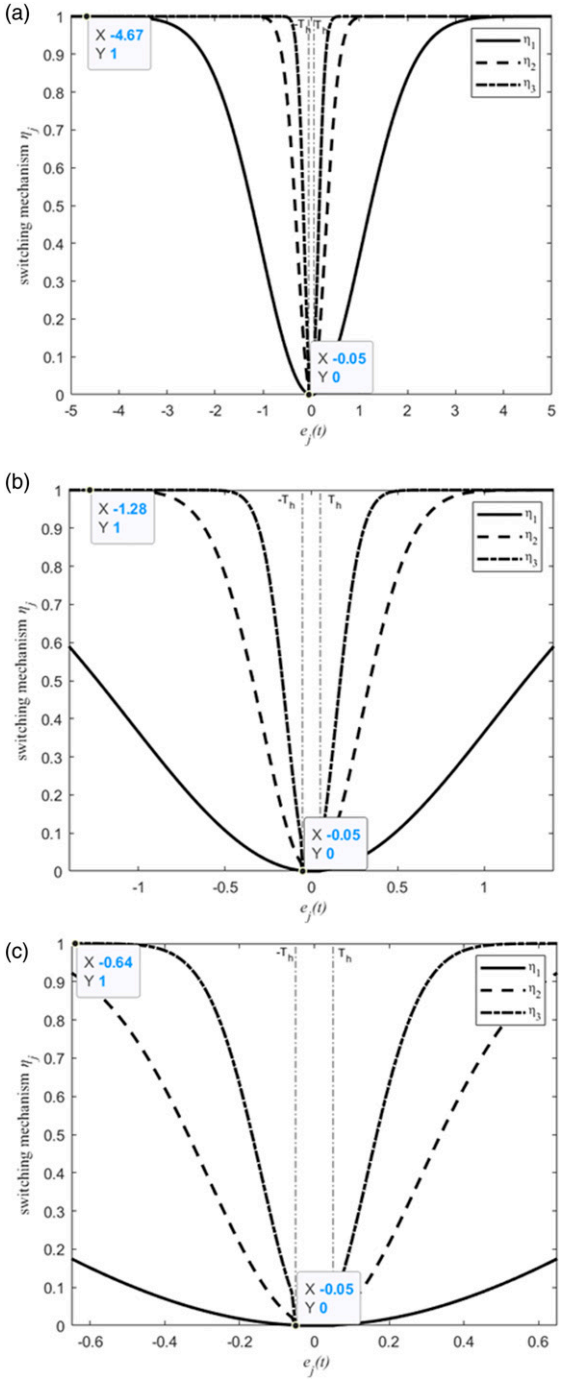

Figure 15. The switching mechanisms for the MIMO gantry crane system by using RAMPA-based method with tunable CF. (a) magnified for η_1, (b) magnified for η_2, and (c) magnified for η_3.

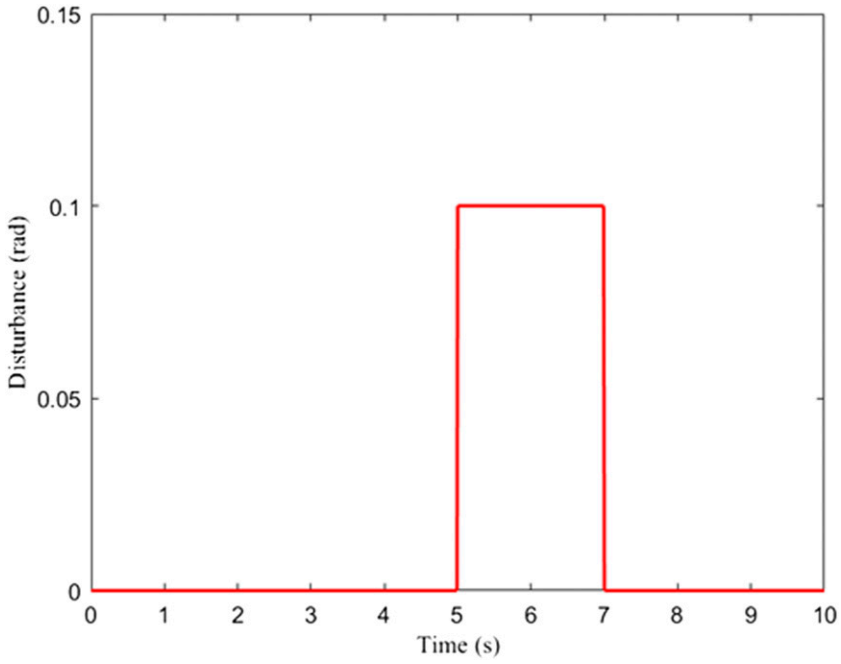

Figure 16. Disturbance signal $d_{y_3}(t)$.

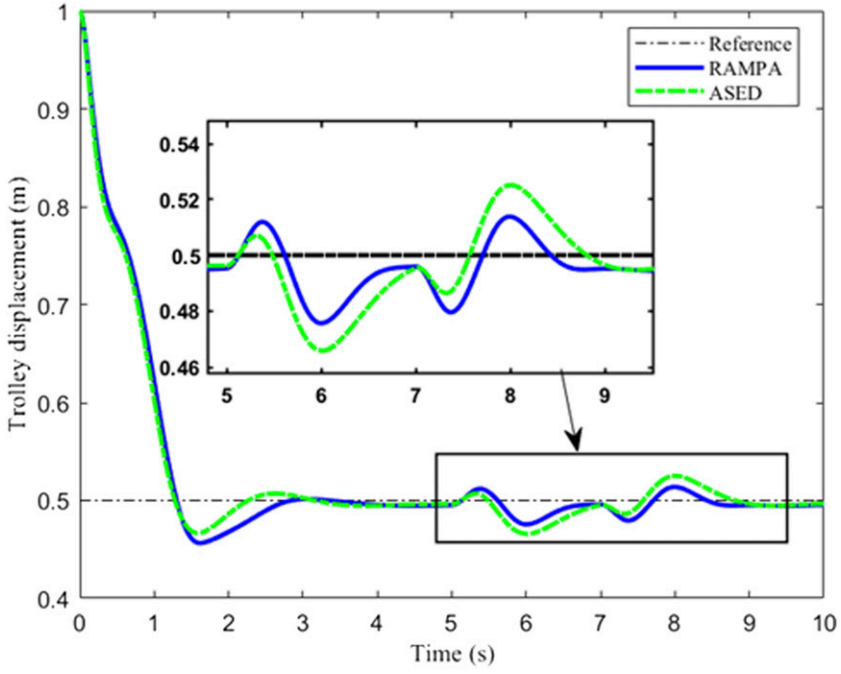

Figure 17. Trolley displacement $y_1(t)$ responses with disturbance.

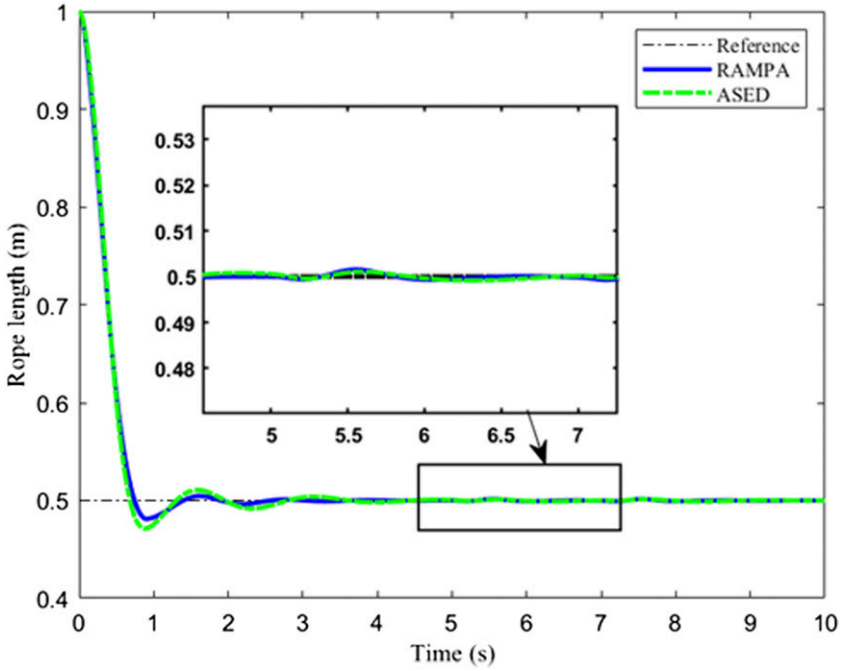

Figure 18. Rope length $y_2(t)$ responses with disturbance.

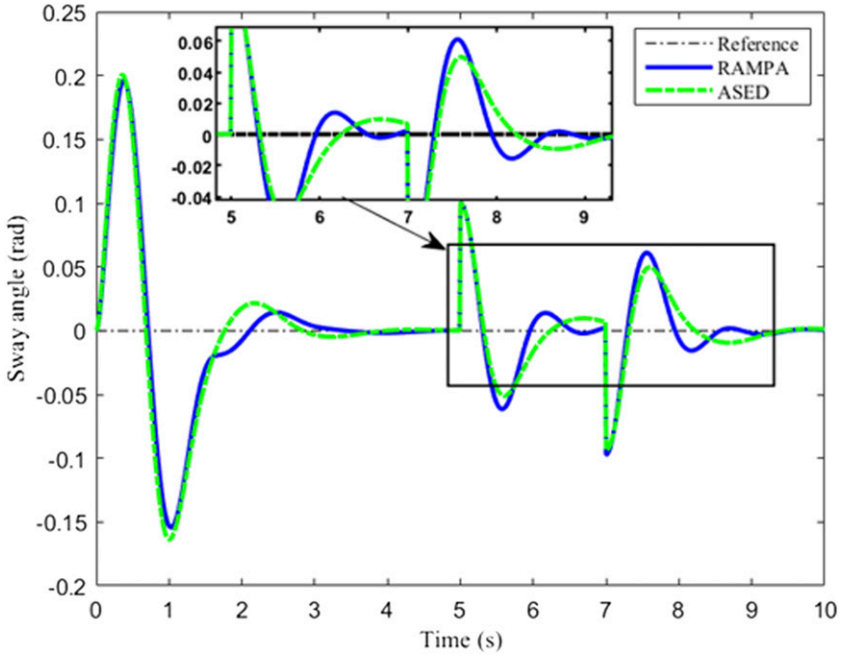

Figure 19. Sway angle $y_3(t)$ responses with disturbance.

$$d_{y_3}(t) = \begin{cases} 0, \text{if } 0 < t < 5, \\ 0.1, \text{if } 5 \leq t \leq 7, \\ 0, \text{if } 7 < t < 10. \end{cases} \tag{36}$$

Registered responses for trolley displacement $y_1(t)$, length of the rope $y_2(t)$, and sway angle $y_3(t)$ of the studied system, alongside their magnified versions amidst crucial oscillations upon encountering interruption of external disturbance, have been independently outlined through Figure 17, 18, and 19. As shown in Figure 17, a smaller oscillation was generated by the RAMPA-based method with tunable *CF* at a shorter recovery interval of 1.6 s following the disturbance, against a settling time of 1.9 s from the former ASED-based method. While similarly unchanged lengths of the $y_2(t)$ have prevailed in Figure 18 for both the investigated algorithms; a marginally smaller sway angle $y_3(t)$ can be observed in Figure 19 for the proposed algorithm over the contending predecessor amidst intervention of the external disturbance. A comparatively diminished settling time of 2 s as recorded for RAMPA-based method with tunable *CF* against an interval of 2.3 s from the ASED-based method has further reaffirmed the former's marginal excellence in uncertainty management. Cumulative results, thus, verified the proposed algorithm as a better approach towards the optimization of MnHR-NEPID controller for the controlling of a MIMO gantry crane system in the presence of external disturbance.

Conclusion

Amidst introducing the RAMPA-based method with tunable *CF* as a contemporary optimization algorithm on the data-driven MnHR-NEPID controller of a MIMO gantry crane system, the current study has fundamentally unearthed three main substantial contributions. Providing an increased withdrawal ability from the local optima, the first contribution hereby confirmed the proposed method as an improvement to the conventional MPA in view of its random average location calculation. The second contribution then contributes an advanced search capability to the conventional MPA by adoption of the tunable *CF* that allows wider users' flexibility in acquiring a balanced degree of exploration and exploitation within the algorithm. Embracing the objective of ameliorating the practicality of a MIMO gantry crane system, this study is ultimately revealed as a founding research which employed multi-agent–based optimization for the fine-tuning of MnHR-NEPID control parameters.

Demonstrated through plotted convergence curves of the average fitness function, RAMPA-based method with tunable *CF* prevailed as the superior approach over its other metaheuristic-based predecessors upon yielding the smallest fitness function. Such eminence is complemented by the method's comparatively superior performance in the aspects of fitness function, as well as the total norms of error and input, in addition to an enhanced accuracy as confirmed through the conducted Wilcoxon's rank test and box plot statistics. A considerably diminished settling time for trolley displacement, percentage overshoot of the rope's length, maximum magnitude of the sway angle, as well as range of the recorded input force against performance of the formerly published ASED-based algorithm has further established a better time response on the proposed method. Such has also been the case when it comes to counteracting adversities brought about by the experimented disturbance.

In accounts of both feasibility and vast applicability of the RAMPA-based method with tunable *CF*, the proposed method holds promising potential in actual implementations of numerous control applications. However, the method's sole excellence in handling single fitness function is contravened by its deficiency in the concurrent management of multiple fitness functions with contradicting objectives. Upcoming research concern within similar academic context is, therefore, allocated to the examining of multi-objective RAMPA-based method with tunable *CF* for accuracy improvement. This is on the realization that the proposed method can also be investigated towards resolutions of real-time issues as encountered within systems ranging from automatic voltage regulator (AVR) control system, induction motor drive control of an electric vehicle to maneuvering control of a twin-rotor MIMO system, through its alternative implementations within other nonlinear PID controllers.

Acknowledgments

The highest gratitude is especially extended to the Ministry of Higher Education for the financial assistance provided under Fundamental Research Grant Scheme (FRGS) No. FRGS/1/2021/ICT02/UMP/03/3 (University reference RDU 210117).

Declaration of conflicting interests

The author(s) declared no potential conflicts of interest with respect to the research, authorship, and/or publication of this article.

Funding

The author(s) disclosed the receipt of the following financial support for the research, authorship, and/or publication of this article: This work was supported by the Ministry of Higher Education Malaysia (FRGS/1/2021/ICT02/UMP/03/3).

ORCID iDs

Mohd Zaidi Mohd Tumari https://orcid.org/0000-0003-2784-5022
Mohd Riduwan Ghazali https://orcid.org/0000-0002-4602-2251

References

1. Ramli L, Mohamed Z, Abdullahi AM, et al. Control strategies for crane systems: a comprehensive review. *Mech Syst Signal Process* 2017; 95: 1–23. DOI: 10.1016/j.ymssp.2017.03.015
2. Madhekar SN and Jangid RS. Variable dampers for earthquake protection of benchmark highway bridges. *Smart Mater Struct* 2009; 18(11): 115011. DOI: 10.1088/0964-1726/18/11/115011
3. Kataria NP and Jangid RS. Seismic protection of the horizontally curved bridge with semi-active variable stiffness damper and isolation system. *Adv Struct Eng* 2016; 19(7): 1103–1117. DOI: 10.1177/1369433216634477
4. Nguyen VT, Yang C, Du C, et al. Design and implementation of finite time sliding mode controller for fuzzy overhead crane system. *ISA Trans* 2019; 124. DOI: 10.1016/j.isatra.2019.11.037
5. Li C, Xia Y and Wang W. H∞ output-feedback anti-swing control for a nonlinear overhead crane system with disturbances based on T-S fuzzy model. *IEEE Access* 2021; 9: 135571–135584. DOI: 10.1109/ACCESS.2021.3115948
6. Yang L and Ouyang H. Precision-positioning adaptive controller for swing elimination in three-dimensional overhead cranes with distributed mass beams. *ISA Trans* 2021; 127. DOI: 10.1016/j.isatra.2021.08.035
7. Wu Q, Wang X, Hua L, et al. Modeling and nonlinear sliding mode controls of double pendulum cranes considering distributed mass beams, varying roped length and external disturbances. *Mech Syst Signal Process* 2021: 158. DOI: 10.1016/j.ymssp.2021.107756
8. Li Y, Zhou S and Zhu H. A backstepping controller design for underactuated crane system. *Proc 30th Chinese Control Decis Conf CCDC* 2018; 2018: 2895–2899. DOI: 10.1109/CCDC.2018.8407619
9. Wang T, Tan N, Zhang X, et al. A time-varying sliding mode control method for distributed-mass double pendulum bridge crane with variable parameters. *IEEE Access* 2021; 9: 75981–75992. DOI: 10.1109/ACCESS.2021.3079303
10. Xiao R, Wang Z, Chen Z, et al. Anti-swing design for overhead crane based on dual sliding mode control. *Proc IEEE Int Conf Ind Technol* 2018; 2018-Febru: 81–86. DOI: 10.1109/ICIT.2018.8352156
11. Aguiar C, Leite D, Pereira D, et al. Nonlinear modeling and robust LMI fuzzy control of overhead crane systems. *J Franklin Inst* 2021; 358(2): 1376–1402. DOI: 10.1016/j.jfranklin.2020.12.003
12. Ouyang H, Zhao B and Zhang G. Enhanced-coupling nonlinear controller design for load swing suppression in three-dimensional overhead cranes with double-pendulum effect. *ISA Trans* 2021; 115: 95–107. DOI: 10.1016/j.isatra.2021.01.009
13. Ouyang H, Tian Z, Yu L, et al. Adaptive tracking controller design for double-pendulum tower cranes. *Mech Mach Theory* 2020; 153: 103980. DOI: 10.1016/j.mechmachtheory.2020.103980
14. Van Trieu P, Cuong HM, Dong HQ, et al. Adaptive fractional-order fast terminal sliding mode with fault-tolerant control for underactuated mechanical systems: application to tower cranes. *Autom Constr* 2021; 123: 103533. DOI: 10.1016/j.autcon.2020.103533
15. Gutierrez I and Collado J. An LQR controller in the obstacle avoidance of a two-wires hammerhead crane. *Neurocomputing* 2017; 233: 14–22. DOI: 10.1016/j.neucom.2016.08.104
16. Wu TS, Karkoub M, Wang H, et al. Robust tracking control of MIMO underactuated nonlinear systems with dead-zone band and delayed uncertainty using an adaptive fuzzy control. *IEEE Trans Fuzzy Syst* 2017; 25(4): 905–918. DOI: 10.1109/TFUZZ.2016.2586970
17. Yang T, Sun N and Fang Y. Adaptive fuzzy control for a class of MIMO underactuated systems with plant uncertainties and actuator deadzones: design and experiments. *IEEE Trans Cybern* 2021; 52(8): 8213–8226. DOI: 10.1109/TCYB.2021.3050475
18. Sun N, Wu Y, Chen H, et al. Antiswing cargo transportation of underactuated tower crane systems by a nonlinear controller embedded with an integral term. *IEEE Trans Autom Sci Eng* 2019; 16(3): 1387–1398. DOI: 10.1109/TASE.2018.2889434
19. Nguyen TL, Nguyen HQ and Duong MD. Payload motion control for a varying length flexible gantry crane. *Automatika* 2021; 62(3–4): 520–529. DOI: 10.1080/00051144.2021.1991176
20. Saeed MU, Sun Z and Elias S. Research developments in adaptive intelligent vibration control of smart civil structures. *J Low Freq Noise Vib Act Control* 2022; 41(1): 292–329. DOI: 10.1177/14613484211032758
21. Song R, Xie Y and Zhang Z. Data-driven finite-horizon optimal tracking control scheme for completely unknown discrete-time nonlinear systems. *Neurocomputing* 2019; 356: 206–216. DOI: 10.1016/j.neucom.2019.05.026
22. Jaafar HI and Mohamed Z. PSO-tuned PID controller for a nonlinear double-pendulum crane system. In: *Communications in Computer and Information Science*. Singapore: Springer, 2017, 752, pp. 203–215. DOI: 10.1007/978-981-10-6502-6_18

23. Sun Z, Bi Y, Zhao X, et al. Type-2 fuzzy sliding mode anti-swing controller design and optimization for overhead crane. *IEEE Access* 2018; 6: 51931–51938. DOI: 10.1109/ACCESS.2018.2869217
24. Sun Z, Zhao X, Sun Z, et al. Optimal sliding mode controller design based on dynamic differential evolutionary algorithm for under-actuated crane systems. *IEEE Access* 2018; 6: 67469–67476. DOI: 10.1109/ACCESS.2018.2872062
25. Solihin MI, Chuan CY and Astuti W. Optimization of fuzzy logic controller parameters using modern meta-heuristic algorithm for gantry crane system (GCS). In: *Materials Today: Proceedings*. Taman Connaught: Elsevier, 2019, 29, pp. 168–172. DOI: 10.1016/j.matpr.2020.05.641
26. Bao HQ, An J, Zhou MC, et al. A Data-driven MPC algorithm for bridge cranes. In: International Conference on Advanced Mechatronic Systems, ICAMechS. Vol 2020-Decem, Hanoi, Vietnam, 10-13 December 2020. IEEE Computer Society, pp. 328–332. DOI: 10.1109/ICAMechS49982.2020.9310150
27. Valluru SK, Kaur M, Kartikeya K, et al. Experimental investigation of fully informed particle swarm optimization tuned multi loop L-PID and NL-PID Controllers for gantry crane system. *Procedia Comput Sci* 2020; 171: 130–138. DOI: 10.1016/J.PROCS.2020.04.014
28. Roman RC, Precup RE, Petriu EM, et al. Model-free adaptive control with fuzzy component for tower crane systems. *Conf Proc - IEEE Int Conf Syst Man Cybern* 2019; 2019: 1384–1389. DOI: 10.1109/SMC.2019.8914376
29. Roman RC, Precup RE, Petriu EM, et al. First-order active disturbance rejection-virtual reference feedback tuning control of tower crane systems. In: 2020 24th International Conference on System Theory, Control and Computing (ICSTCC 2020), Sinaia, Romania, 8-10 October 2020: 137–142. DOI: 10.1109/ICSTCC50638.2020.9259632
30. Roman RC, Precup RE and Petriu EM. Hybrid data-driven fuzzy active disturbance rejection control for tower crane systems. *Eur J Control* 2021; 58: 373–387. DOI: 10.1016/j.ejcon.2020.08.001
31. Pham HA and Soffker D. Improved model-free adaptive control method using recursive least-squares estimation algorithm. *Eur Control Conf* 2020; 2020: 47–52. *ECC 2020*. DOI: 10.23919/ecc51009.2020.9143691
32. Ghazali MR, Ahmad MA, Jusof MFM, et al. A data-driven neuroendocrine-PID controller for underactuated systems based on safe experimentation dynamics. *Proc - 2018 IEEE 14th Int Colloq Signal Process its Appl CSPA* 2018; 2018: 61–66. DOI: 10.1109/CSPA.2018.8368686
33. Ghazali MR, Ahmad MA and Raja Ismail RMT. Adaptive safe experimentation dynamics for data-driven neuroendocrine-PID control of MIMO systems. *IETE J Res* 2019; 68(3): 1611–1624. DOI: 10.1080/03772063.2019.1656556
34. Ghazali MR, Ahmad MA, Raja Ismail RMT, et al. An improved neuroendocrine–proportional–integral–derivative controller with sigmoid-based secretion rate for nonlinear multi-input–multi-output crane systems. *J Low Freq Noise Vib Act Control* 2020; 39(4): 1172–1186. DOI: 10.1177/1461348419867524
35. Ghazali MR, Ahmad MA and Raja Ismail RMT. A multiple-node hormone regulation of neuroendocrine-PID (MnHR-NEPID) control for nonlinear MIMO systems. *IETE J Res* 2020; 68(6): 4476–4491. DOI: 10.1080/03772063.2020.1795939
36. Faramarzi A, Heidarinejad M, Mirjalili S, et al. Marine predators algorithm: a nature-inspired metaheuristic. *Expert Syst Appl* 2020; 152: 113377. DOI: 10.1016/j.eswa.2020.113377
37. Elminaam DSA, Nabil A, Ibraheem SA, et al. An efficient marine predators algorithm for feature selection. *IEEE Access* 2021; 9: 60136–60153. DOI: 10.1109/ACCESS.2021.3073261
38. Aly M, Ahmed EM, Rezk H, et al. Marine predators algorithm optimized reduced sensor fuzzy-logic based maximum power point tracking of fuel cell-battery standalone applications. *IEEE Access* 2021; 9: 27987–28000. DOI: 10.1109/ACCESS.2021.3058610
39. Soliman MA, Hasanien HM and Alkuhayli A. Marine predators algorithm for parameters identification of triple-diode photovoltaic models. *IEEE Access* 2020; 8: 155832–155842. DOI: 10.1109/ACCESS.2020.3019244
40. Elaziz MA, Ewees AA, Yousri D, et al. An improved marine predators algorithm with fuzzy entropy for multi-level thresholding: real world example of COVID-19 CT image segmentation. *IEEE Access* 2020; 8: 125306–125330. DOI: 10.1109/ACCESS.2020.3007928
41. Yakout AH, Attia MA and Kotb H. Marine predator algorithm based cascaded PIDA load frequency controller for electric power systems with wave energy conversion systems. *Alexandria Eng J* 2021; 60(4): 4213–4222. DOI: 10.1016/j.aej.2021.03.011
42. Yakout A, Sabry W and Hasanien HM. Enhancing rotor angle stability of power systems using marine predator algorithm based cascaded PID control. *Ain Shams Eng J* 2021; 12(2): 1849–1857. DOI: 10.1016/j.asej.2020.10.018
43. Sobhy MA, Abdelaziz AY, Hasanien HM, et al. Marine predators algorithm for load frequency control of modern interconnected power systems including renewable energy sources and energy storage units. *Ain Shams Eng J* 2021; 12(4): 3842–3857. DOI: 10.1016/j.asej.2021.04.031
44. Shukla A and Gupta AK. Damping enhancement of DFIG integrated power system by coordinated controllers tuning using marine predators algorithm. *Lect Notes Electr Eng* 2021; 710: 165–176. DOI: 10.1007/978-981-15-8815-0_15
45. Humphries NE, Queiroz N, Dyer JRM, et al. Environmental context explains Levy and Brownian movement patterns of marine predators. *Nature* 2010; 465(7301): 1066–1069. DOI: 10.1038/nature09116
46. Jui JJ and Ahmad MA. A hybrid metaheuristic algorithm for identification of continuous-time Hammerstein systems. *Appl Math Model* 2021; 95: 339–360. DOI: 10.1016/j.apm.2021.01.023

47. Park MS, Chwa D and Eom M. Adaptive sliding-mode antisway control of uncertain overhead cranes with high-speed hoisting motion. *IEEE Trans Fuzzy Syst* 2014; 22(5): 1262–1271. DOI: 10.1109/TFUZZ.2013.2290139
48. Eberhart R and Kennedy J. New optimizer using particle swarm theory. In: Proceedings of the International Symposium on Micro Machine and Human Science, Nagoya, Japan, 4-6 October 1995. DOI: 10.1109/mhs.1995.494215
49. Mirjalili S, Mirjalili SM and Lewis A. Grey wolf optimizer. *Adv Eng Softw* 2014; 69(2014): 46–61. DOI: 10.1016/j.advengsoft.2013.12.007
50. Mirjalili S. Moth-flame optimization algorithm: a novel nature-inspired heuristic paradigm. *Knowledge-Based Syst* 2015; 89: 228–249. DOI: 10.1016/j.knosys.2015.07.006
51. Mirjalili S, Mirjalili SM and Hatamlou A. Multi-verse optimizer: a nature-inspired algorithm for global optimization. *Neural Comput Appl* 2016; 27(2): 495–513. DOI: 10.1007/s00521-015-1870-7
52. Mirjalili S. SCA: a sine cosine algorithm for solving optimization problems. *Knowledge-Based Syst* 2016; 96: 120–133. DOI: 10.1016/j.knosys.2015.12.022
53. Mirjalili S, Gandomi AH, Mirjalili SZ, et al. Salp swarm algorithm: a bio-inspired optimizer for engineering design problems. *Adv Eng Softw* 2017; 114: 163–191. DOI: 10.1016/j.advengsoft.2017.07.002
54. Li S, Chen H, Wang M, et al. Slime mould algorithm: a new method for stochastic optimization. *Futur Gener Comput Syst* 2020; 111: 300–323. DOI: 10.1016/j.future.2020.03.055
55. Karami H, Anaraki MV, Farzin S, et al. Flow direction algorithm (FDA): a novel optimization approach for solving optimization problems. *Comput Ind Eng* 2021; 156(October 2020): 107224. DOI: 10.1016/j.cie.2021.107224
56. Suid MH and Ahmad MA. Optimal tuning of sigmoid PID controller using nonlinear sine cosine algorithm for the automatic voltage regulator system. *ISA Trans* 2021; 128(Part B): 265–286. DOI: 10.1016/j.isatra.2021.11.037

Appendix

Abbreviations

MPA	Marine predators algorithm
RAMPA	Random average marine predators algorithm
CF	Adaptive coefficient to control step size
PID	Proportional-integral-derivative
PI	Proportional-integral
PIDA	Proportional-integral-derivative-acceleration
NEPID	Neuroendocrine-PID
SbSR-NEPID	Sigmoid-based secretion rate neuroendocrine-PID
MnHR-NEPID	Multiple-node hormone regulation neuroendocrine-PID
SISO	Single-input–single-output
SIMO	Single-input-multi-output
MIMO	Multi-input–multi-output
PSO	Particle swarm optimization
GWO	Grey wolf optimizer
MFO	Moth-flame optimization
MVO	Multi-verse optimizer
SCA	Sine-cosine algorithm
SSA	Salp-swarm algorithm
SMA	Slime mould algorithm
FDA	Flow direction algorithm
ASED	Adaptive safe experimentation dynamics
LMI	Linear matrix inequalities
LQR	Linear quadratic regulator
ADE	Adaptive differential evolutionary
DDE	Dynamic differential evolutionary
SMC	Sliding mode controller
CS	Cuckoo search
DE	Differential evolution
BO	Bayesian optimizer
MPC	Model predictive controller

FIPSO	Fully informed particle swarm optimization
MFAC	Model-free adaptive control
PDTSFC	Proportional-derivative Takagi–Sugeno fuzzy controller
ADRV-VRFT	Active disturbance rejection-virtual reference feedback tuning
RLS	Recursive least-squares
PA	Projection algorithm
k-NN	k-Nearest Neighbors
MPPT	Maximum power point tracking
TDPV	Triple-diode photovoltaic
PV	Photovoltaic
MLT	Multi-level threshold